Simulation of Post-fire Watershed Hydrology and Erosion Responses with the Physically-based WEPP Model

A Thesis
Presented in Partial Fulfilment of the Requirements for the
Degree of Master of Science
with a
Major in Water Resources
in the
College of Graduate Studies
University of Idaho
by

Dylan S. Quinn

Major Professor: Erin S. Brooks, Ph.D.
Committee Members: Peter R. Robichaud, Ph.D.; Roger Lew, Ph.D.
Department Administrator: Robert Heinse, Ph.D.

December 2018

Authorization to Submit Thesis

This thesis of Dylan Quinn, submitted for the degree of Master of Science with a Major in Water Resources and titled "Simulation of Post-fire Watershed Hydrology and Erosion Responses with the Physically-based WEPP Model," has been reviewed in final form. Permission, as indicated by the signatures and dates below, is now granted to submit final copies to the College of Graduate Studies for approval.

Major Professor:

Erin S. Brooks, Ph.D.	Date

Committee Members:

Peter R. Robichaud, Ph.D.	Date
Roger Lew, Ph.D.	Date

Department Head:

Robert Heinse, Ph.D.	Date

Abstract

The cascading consequences of fire-induced ecological changes have profound impacts on both natural and managed forest ecosystems. In many areas, natural and human-caused wildland fire are becoming more prevalent due to historical management practices and exacerbated by climate change. Post-fire soil erosion and runoff have been closely linked with the severity of the wildfire, and forest managers tasked with implementing mitigation strategies need robust tools to evaluate the effectiveness of their decisions, particularly those affecting hydrological recovery. Various hillslope-scale interfaces of the physically-based Water Erosion Prediction Project (WEPP) model have been successfully validated for this purpose using fire-affected plot experiments, however these interfaces are explicitly designed to simulate single hillslopes. Spatially-distributed, catchment-scale WEPP interfaces have been developed over the past decade, however none have been validated for post-fire conditions, posing a barrier to adoption for forest managers. Within, a new processing framework is described which enhances the ability of the spatial WEPP model to capture hillslope-scale patterns in soil burn severity. This framework is first assessed using a large post-fire watershed with 163 discrete hillslopes. Compared to the default WEPP processing method, 59% of the hillslopes in the catchment saw a change in magnitude greater than 1 Mg ha^{-1} yr^{-1}. These methods are then applied to compare simulations results with five years of post-fire runoff and erosion observations for a 117-ha forested watershed after the 2011 Wallow Fire in Eastern Arizona. After calibration, the model accurately described daily streamflow for the first two years after the fire (Nash-Sutcliffe Efficiency, NSE; 0.70 – 0.75). Peak streamflow was slightly underpredicted for the first year after the fire while consequent years were well captured. For the first and second years after the fire the largest daily peak flows were simulated at 54.1 and 74.8 mm day^{-1} (NSE 0.30 and 0.76; r^2 0.60 and 0.78). Both hillslope erosion rates and watershed sediment yield were similarly well described by the model for this period (r^2; 0.73 and 0.82). For the first year, this resulted in high soil burn severity hillslope erosion rates of 70 - 85 Mg ha^{-1} and a total catchment sediment yield of 2.7 Mg ha^{-1} yr^{-1}. This calibrated model was further applied to a nearby 207-ha catchment and performed well (NSE; 0.57). Lastly, visualization strategies are developed to represent spatial WEPP processing structures which facilitate usability and adoption of such models.

Acknowledgements

This work would not have been possible without the assistance, generosity, scrutiny, and thoughtful conversations from a wonderful academic community. My major professor, Dr. Erin Brooks, has been endlessly helpful in guiding my pursuits and I am extremely grateful for all the opportunities he has afforded throughout this graduate program. His extraordinary ability to be both a modeler and a field scientist helped me learn far more than I expected to. I do, however, resent that I still cannot beat him one-on-one on the soccer pitch.

I would like to thank my committee members, Dr. Peter Robichaud and Dr. Roger Lew, for their dedication and assistance to my project and career. Pete continually pushed me into new experiences and opened my eyes to the world of post-fire erosion. I am extremely privileged to have invited many field trips to see firsthand, how we quantify soil erosion and parameterize models. Roger has been continuously helpful in developing the ideas and code used in my project and has also helped tremendously through developing a new WEPP interface framework.

There are a number of scientists, engineers, and researchers at the US Forest Service, Rocky Mountain Research Station who have been exceedingly helpful to this project. I would like to thank Dr. Joe Wagenbrenner for providing the observed datasets used in the modeling exercise in Chapter 3, as well as the larger group of folks who helped collect these data. I would also like to thank Bob Brown and Matt Lesiecki for taking me out to the Wallow Fire in Arizona, as well as Bob's further help in cleaning and interpreting the data. The whole team at the RMRS has been delightful to work with both in and out of the field.

My time at the University of Idaho would not have been as exciting or enlightening without the help of the great faculty, staff, and peers in the Soil and Water Systems department and the Water Resources Program. I would like to thank Dr. Mariana Dobre for putting up with me as am office mate for the last two years, as well as offering a great deal of expertise with the WEPP model. I am extremely grateful of the larger FireEarth group, which has enlightened me to the inner workings of an interdisciplinary research project. My work is just a drop in the bucket of the larger picture of fire, and the work by such a large group of world-class researchers has inspired my future ambitions. I would like to specifically thank Dr. Crystal Kolden for her reliable support and generosity throughout my graduate program.

Dedication

To my parent who have provided their unwavering love
and support of all my pursuits throughout my life.

Table of Contents

List of Figures

List of Tables

Chapter 1: Introduction

Rationale Brief

Fire-induced changes in forested watersheds, including decreased vegetative cover and increased soil erodibility, directly impact runoff and erosion processes. Whereas undisturbed forests experience relatively low erosion rates, moderate to high severity burned areas often cause elevated erosion and runoff responses which can decrease water quality, impact aquatic species habitat, and damage infrastructure through flooding and sedimentation. While fire and erosion are both often seen as natural processes, the increasing presence of humans in the wildland environment and proximity to managed forest land creates new elements of risk and responsibility for land managers to consider.

Past fire suppression efforts and climate shifts in the intermountain western forests are expected to increase the frequency and severity of wildfire in the near future, which has direct consequences to controlling hydrologic processes. Land managers have considerable interest in the ability to predict fire-driven erosion and runoff responses in order to direct mitigation efforts effectively and economically. The current generation of physically-based erosion models, namely the Water Erosion Prediction Project (WEPP), have shown to perform adequately for predicting the hillslope-scale responses, and have seen wide application in directing mitigation strategies. To increase the confidence in model performance and accuracy of output, improvements to the model which capture more of the physical processes at play are necessary. Furthermore, upscaling the WEPP model to the watershed-scale has been accomplished and validated for various managed landscapes, yet no robust validation effort has been conducted for describing post-fire erosion and runoff responses at this larger scale. A post-fire, catchment-scale validation of this model is needed to demonstrate the model's utility and ability to simulate post-fire management practices.

Literature Review

Post-Fire Physical Effects

Burn Severity Classification

Wildfire burn severity is commonly defined by the magnitude of above- and below-ground organic matter loss during a fire event (Keeley, 2009). To this extent, burn severity can be used to describe the magnitude of the physical and ecological fire effects. This term can be further refined as soil burn severity, which is restricted surface and below ground impacts, and has greater implications for the post-fire hydrologic response. Typically, burn severity data is collected, analyzed, and verified from a multitude of sources, with the majority of post-fire assessment data being gathered from satellite imagery and ground-verified by emergency response teams (Parsons, et al., 2010).

Remote Sensing

Two suites of readily available, remotely sensed spectral indices are commonly used to describe burn severity and vegetation; the Normalized Burn Ratio (NBR) and the Normalized Differenced Vegetation Index (NDVI) (Key & Benson, 2006).

$$NBR = \frac{(NIR - SWIR)}{(NIR + SWIR)} \qquad NDVI = \frac{(NIR - RED)}{(NIR + RED)} \tag{1.1}$$

where NIR is near-infrared range, $SWIR$ is the shortwave infrared range, and RED is the red spectral range. For the Landsat 7 ETM+ sensor, this corresponds to Band 4 (0.77 - 0.90 μm), Band 7 (2.09-2.35 μm), and Band 3 (0.63-0.69 μm) respectively (USGS, 2017). These indices are often compared over a time periods to produce differenced versions (e.g. differenced NBR, dNBR), which are more effective in determining magnitude of ecological changes. In comparison of the two indices, Hudak, et al. (2007) noted that NBR may perform slightly better than NDVI in burn severity classification, particularly due to the SWIR band which is less sensitive to smoke effects. Furthermore, the SWIR band is more sensitive to vegetation and soil moisture content as well as non-photosynthetic vegetation (Miller & Thode, 2007). Generally, NBR- and NDVI-based indices are more suited towards discerning above ground post-fire changes compared to subsurface effects (Lewis, et al., 2006; Hudak, et al., 2007). This necessitates careful consideration of data sources, collection methodoligies, and overall

validity of burn severity maps as a proxy for changes in below-ground soil characteristics. In general, fire-induced soil changes should not be infered from vegetation-based spectral indicies, however this is often the only information available which describes burn severity distribution.

Soil Heating and Water Repellency

The rapid combustion of organic matter during a wildfire produces a pulse of energy in all directions through radiative, convective, and conductive heat transfer mechanisms (Figure 1.1) (DeBano, 1996). While much of this energy is expelled upwards through radiative and convective processes, a small, but significant portion permeates down into the soil horizons through conduction. Depending on organic matter presence, this can cause an extended heating effect from the smoldering of duff and the organic horizon as well as larger surface debris (DeBano, 1981). Considerable variability in fine surface fuels, duff thickness, and coarse woody debris is often present in pre-fire landscapes, which increases the small-scale spatial complexity observed in post-fire soil burn severity (Robichaud & Miller, 2000). The effects of this soil heating have been well described (Doerr, et al., 2000), and many researchers have refined procedures to classify soil burn severity (Key & Benson, 2006; Parsons, et al., 2010).

Most undisturbed forest soils readily absorb rainfall; however, some soils types may exhibit water repellent properties. These properties are most commonly caused by native hydrophobic compounds formed near the soil surface; largely a product of vegetative decomposition (Doerr, et al., 2009). When the soil surface is heated during a moderate to severe fire, these hydrophobic compounds can volatilize and be redistributed to the atmosphere as well as lower in the soil horizons (Letey, 2001). The relatively cool temperatures at the lower horizons will cause the volatilized compounds to condense on the deeper soil particles, prompting the hydrophobic layer to reform with elevated hydrophobicity. When this layer is present, initial precipitation may penetrate the top layer of soil, mostly comprised of ash and mineral soil, until it reaches the water repellant boundary. At this point, infiltration will be greatly reduced, producing an overland flow response. This process of soil heating-induced water repellency is generally well understood, as reviewed by Doerr, et al. (2000).

Soil Sealing and Water Content

The infiltration rate can also be affected at the soil surface due to the residual ash layer (Cerdà & Robichaud, 2009). After an initial period, ash can fill the macropores of a soil profile, temporarily reducing infiltration rates. This mechanism is temporally sensitive, and many studies do not capture the full nature of how ash affects infiltration. Directly following a fire, the ash can often increase infiltration rates and increase overall soil water storage by providing a 'cushion' which distributes water through the less dense ash layer (Cerdà & Robichaud, 2009). Post-fire wind and precipitation events can remove these ash pockets before field monitoring equipment is in place, which can be a limiting factor for some studies which may not capture the initial increased infiltration and water storage provided ash.

Changes in soil porosity and bulk density are similarly driven by the presence of ash as well as the collapse of larger aggregates which compact and infiltrate into pore space (Giovannini & Lucchesi, 1997). This pore sealing implicitly decreases the total water holding capacity of the soils and contributes to decreases in infiltration rates (Certini, 2005). Moody et al. (2016) examined the effects of fire intensity on these hydrologically sensitive properties including bulk density, water content, particle size, and organic matter content and noted significant changes in these properties relating to remotely sensed burn severity. Ebel (2012) similarly noted these trends in which the water holding capacity of burned soils were dramatically lower than that of unburned soils, largely attributed to reduction in organic matter and ash-based pore sealing.

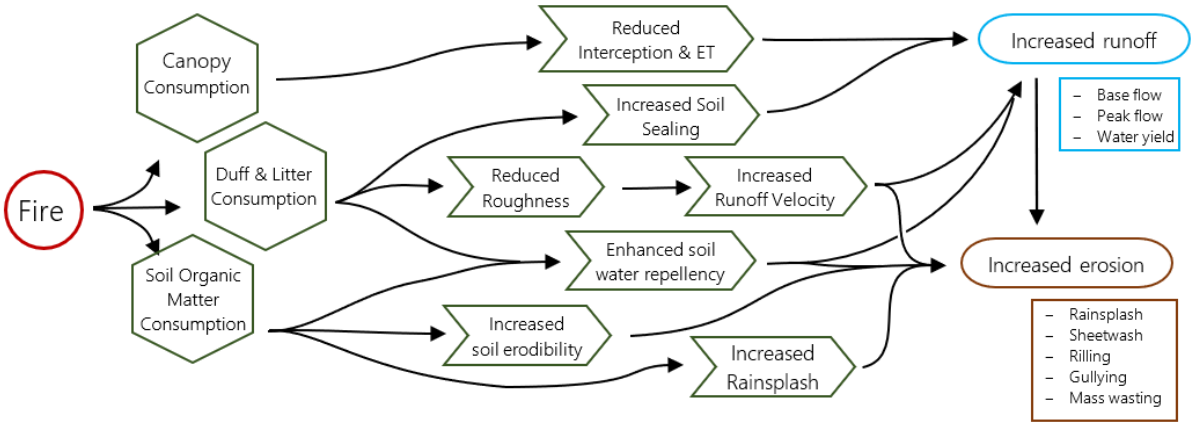

Figure 1.1 Conceptual overview of fire effects on runoff and erosion processes in forested ecosystems. Adapted from Wagenbrenner (2013).

Topographic Influence on Burn Severity

Topographic indices which describe relative aspect, slope, and elevation, as well as various parameters influenced by topography, have been shown to be strongly correlated to burn severity (Dillon, et al., 2011). Birch et al. (2015) noted that topographic parameters are important for determining burn severity at both small and large spatial scales. The mechanisms which drive this interaction are related to the varying levels of fuel loading, fuel moisture content, and population composition (Agee, 1996). For example, topographic aspect in the Northern hemisphere promotes high solar radiation loading on south facing slopes, which are often dryer than north facing slopes and have reduced vegetation and fuel loading (Holden & Jolly, 2011). Further, the relative topographic position (e.g. valley, mid-slope, ridge) has been shown to influence relative humidity and moisture, both of which control ground fuel combustion processes (Dillon, et al., 2011). Topographic wetness, or the gradient of soil water content relative to topographic position, can also impact both the rate of fuel growth and loading as well as the fuel moisture content. Holden et al. (2009) used these varying topographic indices to create predictive models describing burn severity, and found the mechanisms described above to be consistent with field observations. Dillon, et al. (2011) further documented the influence of steep biophysical gradients in montane ecosystems on burn severity at larger scales, while suggesting hillslope-scale topography can be an important controlling factor.

Spatial Heterogeneity

Physical and ecological fire effects caused by variable patterns in weather, vegetation, and topography are prevalent in all wildfires at differing scales (Lentile, et al., 2006). The unique mosaics of pre-fire conditions including canopy and ground fuel loading, vegetation composition, topographic profiles, and fuel moisture have been suggested as the primary indirect factors influencing post-fire effects and burn severity (Bigler, et al., 2005; Dillon, et al., 2011; Birch, et al., 2015). The spatial scale at which these properties are assessed is important when considering the mechanism of the process in question. For example, at the hillslope-scale of 100 – 500 m, heterogeneity in crown consumption may be highly uniform, contrasted with the fine-scale variability of 1 cm to 1 m commonly seen with duff and liter consumption, and consequently soil water repellency (Robichaud & Miller, 2000).

The spatial resolution of remotely sensed imagery and burn severity maps are often constrained to the coarsest resolution of its inputs; commonly 30 m pixels (e.g. Landsat) While some biophysical mechanisms may be described on this scale, the small-scale heterogeneity inherent in post-fire soil properties, including infiltration, hydraulic conductivity, and water repellency, which can vary widely on a hillslope scale from 0.1 to 100 meters, has profound implications for post-fire hydrological effects (Letty, 2005; Robichaud, et al., 2007).

Watershed Scale Hydrological Modeling

The WEPP Model

The Water Erosion Prediction Project (WEPP) model is a deterministic processes-based sediment transport model which incorporates climatic, topographic, and edaphic data as well as land cover management to estimate soil loss, erosion, and hydrology at the hillslope scale (Flanagan & Nearing, 1995). By using representative rectangular hillslopes based on hillslope area and length of its associated stream segment, the WEPP model can simulate infiltration, surface runoff, lateral flow, soil detachment, transport, and deposition along the slope profile as well as plant growth and decomposition dynamics. At the hillslope scale, the model allows inputs to be defined for soil and land cover for up to 19 distinct segments or overland flow elements (OFEs). This function provides many benefits for processing, including accurate descriptions of vegetation properties along a hillslope, as well as a more appropriate runoff-subsurface flow characterization. Through the GIS interface, GeoWEPP, watershed input files for WEPP can be created for a defined upstream contributing area which allow the model to simulate similar mechanisms within a channel network for a defined watershed (Renschler, 2003; Brooks, et al., 2016). This process allows the model to simulate hillslope sediment transport and watershed sediment and streamflow for catchments on the order of thousands of hectares in size. Compared to the empirically-based Universal – and Revised Universal Soil Loss Equations (USLE and RUSLE) models, WEPP is predominantly process-based which is necessary for applying the model on a watershed scale (Renschler, 2003).

Originally developed as a tool to assess agricultural and rangeland erosion, WEPP has been adapted for suitability in small forested watersheds where model output agrees with field

observations (Dun, et al., 2009). The validity of output at this scale has been further evaluated by Brooks, et al. (2016) who found similar agreement between model output and field observations for large, snow-dominated watersheds. The few validation studies that have been conducted show, at least, the applicability of WEPP to watersheds of increasing size, however, many authors have described the challenges of increasing spatial scope while preserving the hydrological mechanisms at play within the model (Grayson, et al., 1992; Flanagan, et al., 2013). Primarily, stream-routing routines lack robust mechanisms for modeling large networks, reducing accuracy of sediment transport estimations when increasing watershed area (Wang, et al., 2010). Further, spatial heterogeneity of input parameters including soils, vegetation, and small-scale variations in weather and climate may impact the validity of model output if not addressed (Brooks, et al., 2016).

Although the application and validation of WEPP and GeoWEPP models for forested watersheds has been the target of many studies, few authors have attempted watershed-scale validation of post-fire runoff and erosion responses in forested watersheds with the GeoWEPP model (Miller, et al., 2011). Many hillslope interfaces of WEPP including the Erosion Risk Management Tool (ERMiT, Robichaud, Elliot, Pierson, Hall, & Moffet, 2007), and the online Disturbed WEPP interface (Elliot, 2004), have been validated using hillslope-scale plot studies and suggest that WEPP can provide reasonable post-fire predictions at the hillslope scale. Larsen and MacDonald (2007) compared the Disturbed WEPP model with the Revised Universal Soil Loss Equation (RUSLE) against observations for nine fires in the Colorado Front Range and found that WEPP performed slightly better than RUSLE at estimating hillslope erosion with r^2 values ranging between 0.53 to 0.65. Their analysis concluded that WEPP tended to overpredict small events and underpredict large events. Robichaud, Elliot, Lewis, and Miller (2016) conducted a hillslope validation analysis of the probabilistic ERMiT WEPP interface and found the predictions to be ‘reasonable and defensible.’ When comparing post-fire treatments, the model predicted sediment yields on the same order of magnitude as observed values. Both studies recommended that further validation is appropriate to evaluate performance over a range of conditions.

TOPAZ

The GeoWEPP model relies on the Topographic Parameterization (TOPAZ) digital elevation model analysis tool to delineate stream channels, hillslopes, and catchment boundaries (Garbrecht & Martz, 1999). This tool characterizes the slope profile for each hillslope and channel segment required for each WEPP rectangular hillslope and channel representations. TOPAZ uses a simple D8 flow direction algorithm with pre-processing DEM filling and correction with a critical source area (CSA) and minimum stream length threshold for stream delineation. The process provides some control over hillslope size for most landscapes, however several assumptions in the model exist, and may have severe implications for its usage. Namely, the CSA threshold, which is often calibrated to first order streams, can introduce undesirable downstream delineation artifacts which are not representative of real conditions (Garbrecht & Martz, 1999). Further, and possibly more influential in post-fire WEPP simulations, the hillslopes natively generated through the GeoWEPP interface with this tool provide a single slope OFE characterization which allows only a single input of each type to define a hillslope.

Integrating Research Question

The nature of fields in the environmental sciences necessitates an interdisciplinary approach to answer complex analytical questions. Consequently, our driving scientific questions should be designed to address such complexities by examining systems as a whole. Similarly, in their synthesis of post-fire erosion advances, Shakesby et al. (2016) enumerate three guiding recommendations for post-fire modeling; incorporate spatial variability, make models transferable, and improve predictions for emergency responders and managers. With these goal in mind, the following integrating research question was developed to drive the methods and exploration process of post-fire hydrological modeling presented here:

How can process based, watershed-scale hydrological models better inform prevention and remediation strategies of post-fire runoff and erosion in montane forested ecosystems?

Research Goals

The following research goals were designed to address the integrating research question:

- Assess the influence of **hillslope-scale spatial variability in burn severity** on post-fire runoff and erosion using the WEPP watershed model
- Apply and validate the WEPP watershed model to **characterize watershed-scale post-fire runoff and erosion** patterns using observed data
- Develop data **visualization and communication methods** to effectively communicate post-fire runoff and erosion risk with primary fire responders, forest managers, and community stakeholders

These three goals support the overarching integrating research question through an interdisciplinary approach. The first two goals regarding the spatial variability of burn severity and WEPP assessment are disciplinarily based in the fields of hydrology and fire ecology, which will require methods from both to understand the interactions between the physical fire effects and the erosion responses. Developing methods to address the spatially heterogeneous nature of fire severity patterns within the WEPP model will increase the confidence of the model through rigorous hypothesis testing and theory validation. Addressing the integrating question will however, require disciplines outside of the environmental sciences. This is accomplished through the third goal in the development of data visualization and communication methods for risk communication. This element is based in the social sciences and requires techniques from the visual arts, computer sciences, and social psychology to address the needs of land managers and other end-users of this data.

Outline of Chapters

The following three chapters address each of the described research goals. Chapter 2 provides a framework for addressing post-fire, hillslope-scale variability in burn severity within the WEPP model and a general assessment of its impact on WEPP simulations. Chapter 3 describes and discusses the application and validation of this framework to a small watershed in Eastern Arizona. Here, the model is applied for a five-year post-fire period and model results are compared to observed values for streamflow and sediment yield at multiple scales. This model is then applied to a nearby catchment without any further calibration to assess its ability to capture post-fire streamflow. Finally, Chapter 3 provides an outline and application of visualization methods required to effectively communicate modeled information to managers.

Chapter 2: Influence of Burn Severity Heterogeneity on Erosion and Runoff

Abstract

Wildfire generally produces a heterogenous burn severity response over forested landscapes which directly controls post-fire hydrology. Whereas severely burned soils often show very low infiltration rates and increased runoff and erosion, unburned or low soil burn severity patches downslope of high burn severity areas have been shown to mitigate this response. This effect is particularly important in hydrological models which may not capture this inherent variability. In this chapter, methods are developed for the physically-based WEPP model to describe the within-hillslope burn severity heterogeneity using the topographic position index. The method is applied to a sub-watershed within a large fire in Arizona. Comparisons between default processing methods and the method described here shows that incorporating burn severity heterogeneity can influence model simulations of runoff and erosion rates by ±100%.

Introduction

Hillslope Hydraulic Connectivity

Identification and routing of overland flow is an important component to hydrological characterizations; particularly in modeled systems (Beck, et al., 1990; Bracken & Croke, 2007). Hillslope hydraulic connectivity, described as hydraulic functional connectivity by Moody et al. (2008), defines the small-scale hydraulic linkages of water transport down topographic gradients. Compared to the term '*hydrological connectivity*,' which provides a larger-scale ecological application, hydraulic connectivity pertains mainly to hillslope to channel flow processes which occur prior to channelization (Pringle, 2003; Hallema, et al., 2017). During wildfire, spatially sporadic burn patterns often lead to disruptions in existing flow paths which have profound impacts on runoff generation. Downslope unburned or low-burn severity patches are commonly observed in the field, and often provide considerable runoff infiltration capacity compared to upslope burned areas (Robichaud & Monroe, 1997). Conversely, a high burn severity area which is near a toe slope may see considerably higher runoff and sediment transport. On this effect, Cawson et al. (2013) found unburned patches

from 5 to 10 meters in length could reduce sediment transport by upwards of 100% when located below a burned area. Similar relationships have been observed regarding stream buffer zones required for post-fire salvage logging operation, where downslope runoff infiltration capacity is well correlated with burn severity, such that high-burn severity areas require a larger buffer zone compared to low-burn severity areas (Bone, 2017). While burn severity has been noted as an important factor in post-fire runoff production and sediment yield, the hydraulic connectivity of burn severity patches may have more significant controls on these post-fire effects, and need to be included in post-fire erosion and runoff models (Shakesby & Doerr, 2006; Cawson, et al., 2013)

Model Description

The Water Erosion Prediction Project (WEPP) model is a physically-based, hillslope-scale hydrological model which can simulate many processes including infiltration, sub-surface flow, overland flow, soil detachment, transport, and deposition, and vegetation growth and decomposition (Flanagan & Nearing, 1995). The model can also simulate catchment-scale hydrology with topologically-linked channel processes to produce estimates of watershed sediment yield and water flow. Through the ArcGIS-based GeoWEPP tool, hillslopes and channels can be generated from digital elevation models, which include descriptions of soil, vegetation, topography, and climate (Renschler, 2003; Flanagan, et al., 2013). Within the WEPP model, hillslopes are represented as 2D rectangular units where the slope is discretized along the profile, however this is held constant along the hillslope width. Due to this, the model is unable to simulate the effects of planform curvature and all model estimates are calculated per unit hillslope width (Boll, et al., 2015). Hillslopes are further able to be separated into discrete overland flow element (OFE) sections which are processed in series with each other, allowing for hydraulic interactions between elements. The GeoWEPP interface is also capable of generating model inputs to emulate ‘grid-based’ processing through the creation of ‘flowpaths.’ In this process, each flow path is represented by a single hillslope with a profile width the same as the DEM cell size. While this allows for a greater level of detail for both input parameters and output visualization, flowpath processing is extremely computationally expensive, and often prohibitive for larger areas.

Weather processes including temperature, precipitation, solar radiation, wind, dew point, and humidity are required to run the WEPP model. One common approach uses weather generated from the stochastic CLIGEN model included in WEPP distributions (Flanagan & Nearing, 1995). CLIGEN uses climate observations from a network of weather stations throughout the United States to produce daily patterns for all required WEPP weather variables and can produce data series upwards of 100 years. This approach allows WEPP to act as a predictive model for future events through providing a realistic distribution of possible weather scenarios to simulate. For modeling past events, these variables can also be discretely input into the model for single events, using breakpoint precipitation series, or with daily values. These approaches are more useful to verify, validate, or otherwise test hypotheses about the model and simulated hydrologic processes.

Addressing Spatial Variability

Many authors have addressed the need to incorporate the spatial variability of WEPP input parameters as well as fire effects dictated by severity, flame length, and residence time, into any spatial WEPP analyses (Elliot & Robichaud, 2011; Miller, et al., 2011). Within-hillslope variability can be easily incorporated using overland flow elements which can be used to distribute different soil and vegetation inputs along single hillslope. Covert (2003) noted that the lack of multiple OFEs in the GeoWEPP-produced files is inadequate for representing such variability. Many WEPP-based erosion interfaces, including the Erosion Risk Management Tool (ERMiT, Robichaud, et al., 2007), and the Disturbed WEPP interface (Elliot, 2004) utilize OFEs to assist in post-fire erosion estimation and can simulate varying soil burn severity conditions, however these interfaces are explicitly directed toward single hillslope simulations and cannot be automatically applied to larger watersheds. To address OFEs in spatial-WEPP applications, Brooks et al. (2016) described methods to modify the GeoWEPP-generated files by separating slope files into 19 OFEs per hillslope, however due to the complexity of assigning accurate management and soil characteristics to each OFE, no changes were made to the input parameters. While it was noted this inclusion did improve the hydrologic characterization of subsurface flow and runoff partitioning, this study did not address hillslope heterogeneity. Similarly, Boll, et al. (2015) suggested the inclusion of OFEs into WEPP is important for simulating flow convergence effects and has significant impacts

of functional processes modeled. Grayson, et al. (1992) warned that in many scenarios, the inherent heterogeneity in model inputs is not negligible and is challenging to incorporate. The inclusion of multiple OFEs into the WEPP spatial framework allows the model to more accurately capture the commonly observed and hydrologically important spatial variability in vegetative cover and soil properties at the hillslope scale. When modeling post-fire systems, such variability has been shown to be a very sensitive driver for runoff and sediment production.

Objectives

The following objectives were designed to examine the effect of including hillslope-scale burn severity patterns in a post-fire spatial WEPP modeling framework:

- Develop methods to assign OFEs and inputs to WEPP hillslopes for spatial applications.
- Assess characteristic variability of hillslope-scale burn severity in a large catchment within the 2011 Wallow Fire, AZ.
- Examine the effects of including OFEs on runoff and sediment yields compared to default WEPP hillslope processing.

Methods

Methods developed in this study were designed to test the effects of simulating hydraulic functional connectivity on post-fire erosion and runoff simulations within the WEPP model framework. Procedures were developed to topographically characterize and assign hillslope inputs within the WEPP model which don't sacrifice processing time. These procedures were applied through a generic processing scheme to a large catchment within the 2011 Wallow Fire boundary in Eastern Arizona (Figure 2.1 and 2.2). A full description of the fire can be found in Chapter 3.

Model Inputs

Model inputs describing soil and vegetation were selected and distributed according to the ground-verified soil burn severity map (USDA Forest Service, 2017). Generic 'fire-affected' sandy-loam soils and post-fire recovery vegetation files for unburned, low, moderate, and high severity were selected similar to those described in the Erosion Risk Management Tool (Table 2.1) (Robichaud, et al., 2014). A single 100-year climate file was

created for the region using the CLIGEN weather generator program based on the nearby Alpine, AZ climate station.

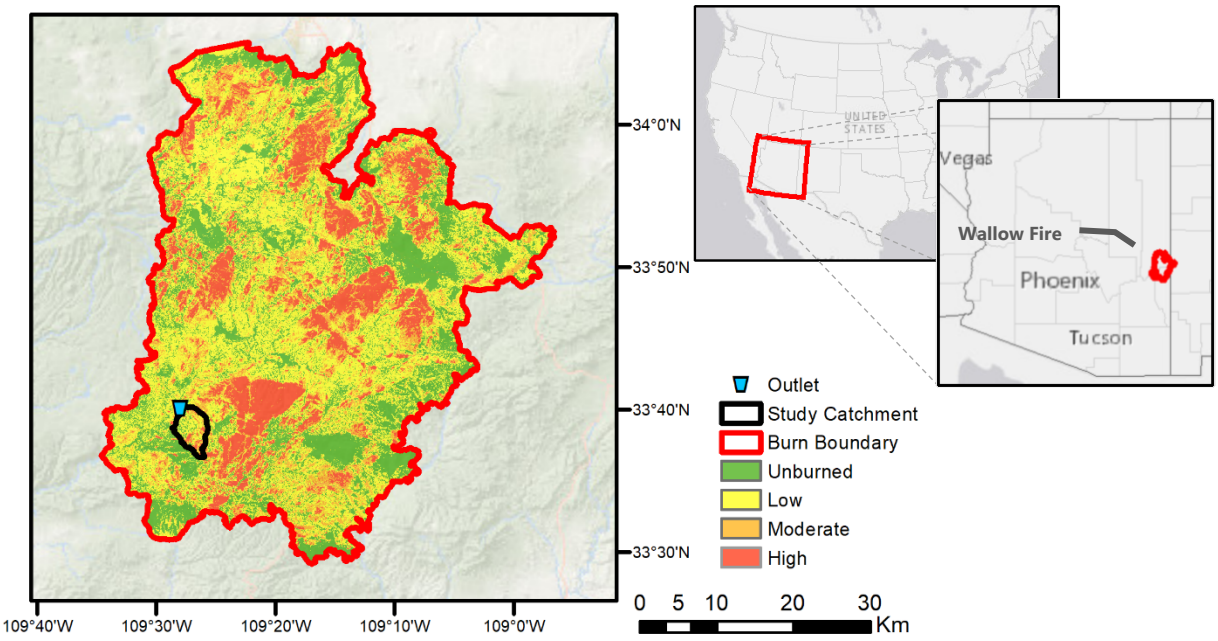

Figure 2.1 Location of the Wallow fire in Eastern Arizona and remotely sensed soil burn severity map.

Table 2.1 Generic forest loam soil properties used to represent each burn severity class (Elliot, 2008).

	Depth	Sand	Clay	Rock	Hydraulic Conductivity	Interrill Erodibility	Rill Erodibility
	mm	%	%	%	mm hr^{-1}	kg s m^{-4}	s m^{-1}
Unb.	800	65	10	5	60	400000	0.00008
Low	400	65	10	5	20	400000	0.00012
Mod	400	65	10	5	20	400000	0.00012
High	400	65	10	5	15	400000	0.00014

Topographic Characterization Process

The Topographic Position Index (TPI) was used to assign distinct OFEs to each hillslope (Weiss, 2001). The index is calculated following:

$$TPI_{scale} = int(z_i - \bar{z}_{focal\_mean,irad,orad}) + 0.5 \quad (2.1)$$

where z_i is the elevation of cell i ; $\bar{z}_{focal\_mean}$ is the annular focal mean of elevation centered around cell i with inner and outer radius of $irad$ and $orad$, and the $scale$ note is equal to the

outer radius (Figure 2.2). For example, TPI_{2000} would be the TPI raster created with an outer radius of 2000 meters. While the range of TPI values can reach extreme values, common autocorrelation in elevation generally ensures the value will be between -100 and 100. Near zero values indicate either a flat zone, or a constant slope feature (e.g. mid-slope), and consequently need to be separated using a flat-slope filter where cells with a zero TPI and slope below a threshold value are reclassified into as flat. (Figure 2.3 a, b). Positive values indicate the cell is located on a ridge top, while negative values indicate the cell is on the valley floor (Figure 2.3 c, d). Following recommendations by Weiss (2001), the TPI raster was classified with 9 groups, including one group for flat areas. Class breaks were selected using the Jenks natural break optimization method (Jenks, 1967).

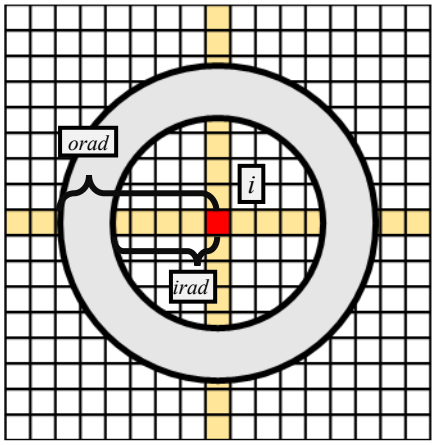

Figure 2.2 Conceptual diagram of the TPI focal area which is used to calculate the annular mean showing inner and outer radius of the annulus for cell *i*

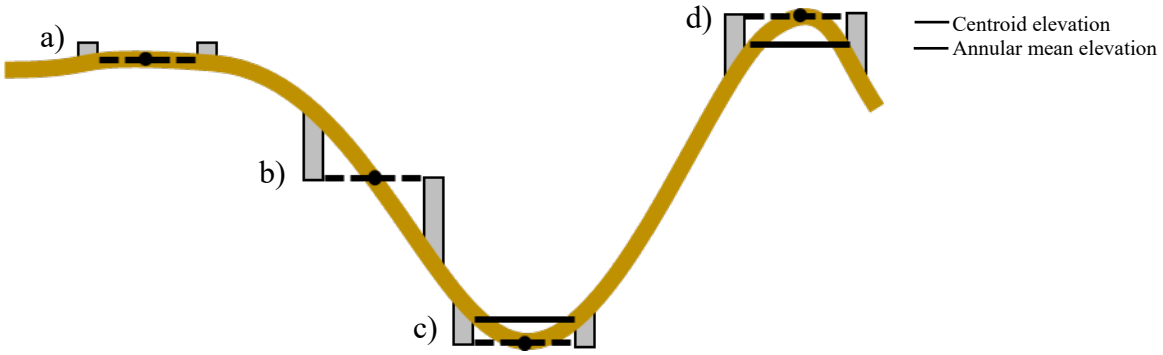

Figure 2.3 Conceptual model of the TPI along a slope profile cross section showing calculations at a) a flat point b) a mid-slope point, c) the valley floor, and d) a ridge. For the mid-slope and flat zone, the average annular mean elevation is approximately equal to the center point elevation, which results in a zero TPI value. Adapted from Weiss (2001)

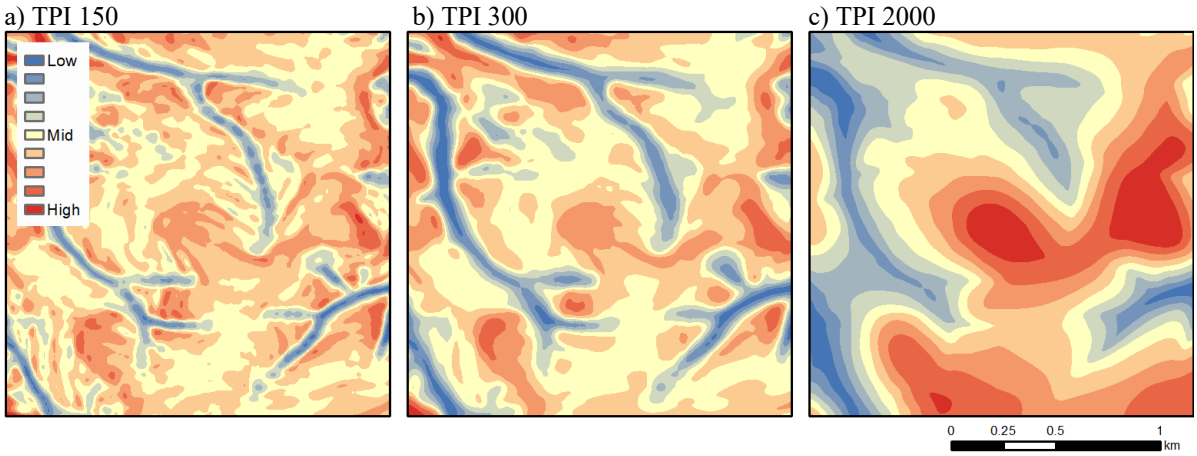

Figure 2.4 TPI rasters produced using a 150-, 300-, and 2000-meter focal radius. As the annular processing radius increases, the output product becomes more generalized and coarser.

This index was chosen over other schemes which may simulate functional connectivity because of its compatibility with the existing automated input processing methods used in online WEPP interfaces as well as the relatively low computing time needed. Other discretization methods were explored including distance-to-stream and relative elevation classification, however these methods often introduced artifacts in the hill segmentation process which introduced unrealistic input characterization. Compared to the existing flowpath processing in GeoWEPP, the methods described here offer the higher resolution of inputs used in flowpath processing with a comparatively minimal computation time.

The classified, 9-band TPI raster was used to select the majority burn severity input in a band for each discrete hillslope. WEPP slope description files, which describe a hill's slope, length, and width, were modified to represenat the 9 bands. A script was created to automatically process these files to include the relative breaks along the slope profile computed using total area occupied within each band following the relation:

$$L_B = \frac{L_T A_B}{A_T} \tag{2.2}$$

where L_B, A_B, L_T and A_T are the length representation of band B, the area represented by band B, the total hillslope representative length, and the total hillslope area, respectively. Soil and management inputs were then assigned based on the majority burn severity classification within each band.

Modeling Framework

Two modeling approaches were compared which included one lumped control and one semi-lumped OFE method. For each method, the watershed boundary and hillslope areas were defined by the GeoWEPP interface using the built-in TOPAZ tool with a critical source area of 5 ha and a minimum source channel length of 100 m. For the study area, this resulted in 163 hillslopes with 56 connecting channels. This process was completed using a 10 m DEM from the National Elevation Dataset (USGS, 2015). A single, 100-year climate file was used for each model run in this simulation. The catchment outlet was arbitrarily chosen for this exercise; however, the selection was made to incorporate a mixture of burn severity classes.

Lumped: Hillslope (>5 ha)

The default GeoWEPP delineation processes was used to delineate hillslope boundaries. This method assigns a single soil type and land cover to the hillslope using a simple majority of burn severity.

Semi-lumped: OFEs (~1 ha, unique soils, management)

This method utilizes the built-in OFEs handled by WEPP. Using the boundaries defined by GeoWEPP, a normalized topographic position index with a 150-meter inner and 300-meter outer radius (TPI 300) was generated for each hillslope, which designated 9 bands of increasing topographic position. From each TPI band within a hillslope, the majority burn severity class (unburned, low, moderate, high) was used to appropriate vegetation and soil inputs.

Results and Discussion

Out of the 163 hillslopes in the study area, 42 hillslopes saw an absolute change greater than 5 mm yr^{-1} between methods (Figure 2.5a). This represented 25% of the total watershed area. Among these hillslopes, almost 75% saw an absolute decrease in runoff. Concerning erosion, 27 hillslopes saw an absolute decrease in average sediment yield greater than 10 Mg ha^{-1} yr^{-1} while 14 hillslopes saw an increase greater than 10 Mg ha^{-1} yr^{-1} using multiple OFE framework (Figure 2.5b). Many of the areas which saw the largest decreases in annual runoff and sediment yield were located near the most severely burned zones in the southern portion of the study region (Figure 2.6b). The default single OFE method described these hillslopes as high burn severity. In contrast, the multiple OFE method often included

moderate, low, or unburned burn severity classifications for these same hillslopes. Conversely, for hillslopes which were originally classified as a less severe burn severity, the multiple OFE method generally increased the erosion rate (Figure 2.6a). In total, 59% of the hillslopes in the catchment saw a change in magnitude greater than 1 Mg ha^{-1} yr^{-1}.

a) Annual Runoff b) Annual Sediment Yield

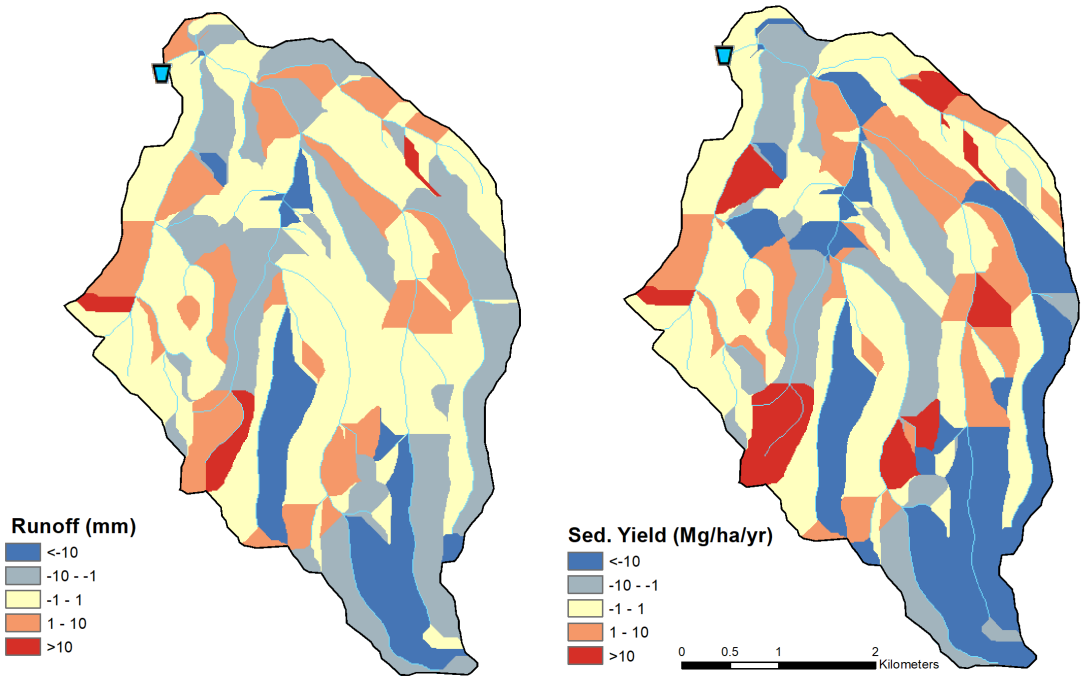

Figure 2.5 Absolute differences in a) annual average runoff and b) sediment yield between single and multiple OFE delineations. Positive values (red) represent a larger average value for the single OFE method compared to the multiple OFE method.

For the entire catchment, the area-weighted hillslope sediment yield rate was 27.3 Mg ha^{-1} yr^{-1} using the single OFE method and 38.3 Mg ha^{-1} yr^{-1} using multiple OFEs representing an increase of 40%. This value is likely site specific, due to the distinct hillslope burn severity patterns of this particular catchment and may differ between fires. While more hillslopes saw a decrease in runoff and sediment yield when using multiple OFEs, the

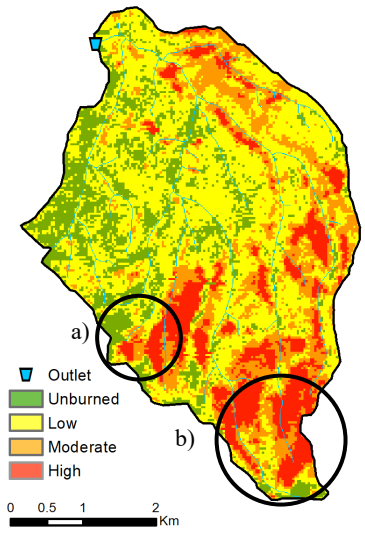

Figure 2.6 Burn severity map of the study area. Highly impacted areas are circled

magnitude of change for hillslopes which saw an increase was generally much higher. This was likely caused by the larger impact of including a small high severity OFE band in a low burn severity hillslope compared to a low burn severity band in a predominantly high severity hillslope. This analysis suggests that capturing the most representative fraction of high burn severity within a hillslope is as, or more, important to total overall simulated sediment load than accurately capturing the unburned or low burn severity fraction. In this example watershed, underrepresentation of high burn severity patches in a mostly low burn severity slope brought about greater error than unaccounted low or no-burn severity patches in a predominantly high burn severity slope.

a) Annual Runoff b) Annual Sediment Yield

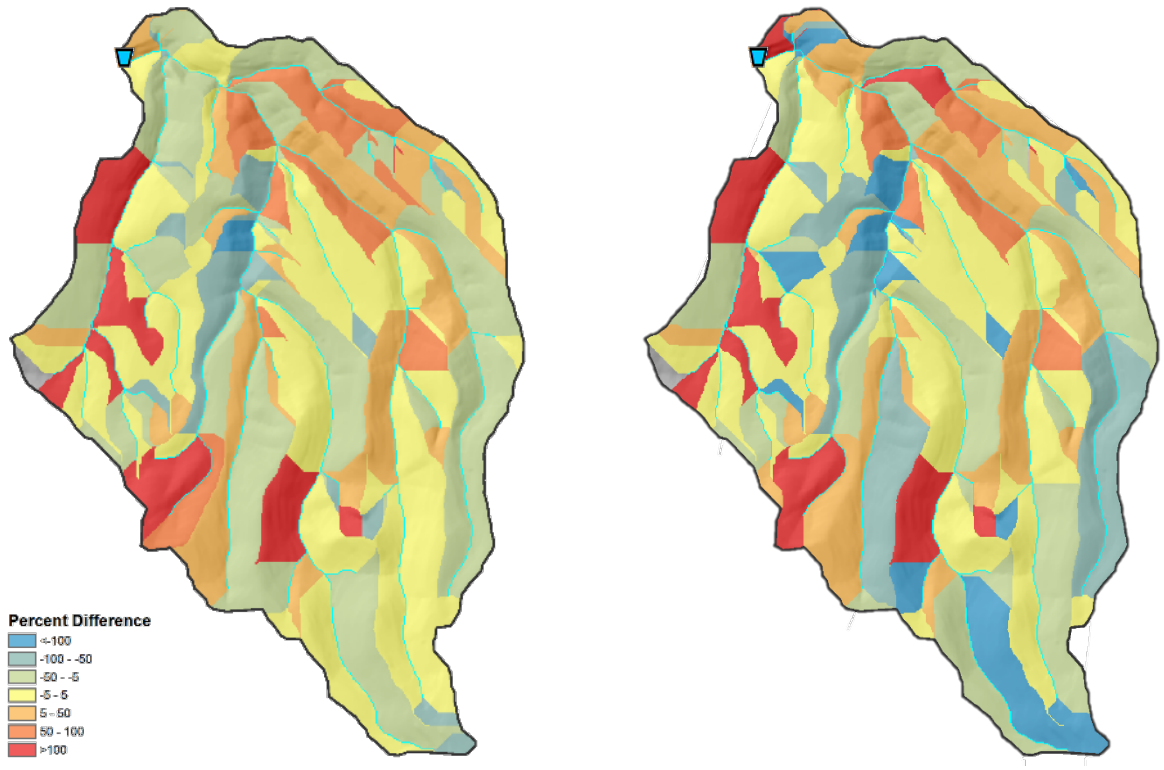

Figure 2.7 Percent difference between single OFE and multiple OFE delineations for a) hillslope sediment yield and b annual runoff for a 100 year simulation period. Positive values indicate an increase in predicted values found using the OFE method

Conclusion

The framework presented here was developed to incorporate a larger degree of spatial variability in soil burn severity into the WEPP model. While many interfaces of the model utilize OFEs to produce this effect, none that do so operate at the watershed scale, and are

instead targeted at hillslope-scale analyses. The topographic position index provides a scale-independent transferable framework to discretize or translate topographic bands to a WEPP representative hillslope using the OFE structure. When this framework was applied to a watershed in the 2011 Wallow Fire, large differences in simulated runoff (> 5 mm yr^{-1}) and sediment yield (>1 Mg ha^{-1} yr^{-1}) were produced in 59% of hillslopes in the catchment. Overall watershed average sediment yield was 40% greater using the OFE structure indicating that the greater error in this watershed was produced by the underrepresentation of minor high burn severity patches within a mostly low burned slope. These large spatial differences in runoff and erosion suggest that decision support tools for targeting hillslopes which contribute the greatest soil erosion should account for spatial patterns in burn severity. This is not only important for capturing downslope infiltration and deposition in a mostly high burn severity slope with a minor low burn severity patch, but it is equally or more important to capture a minor high burn severity patch in a predominantly low burn severity slope.

Chapter 3: Catchment Scale Assessment of a Post-fire, Physically-based, Runoff and Erosion Model

Abstract

With an expected increase in wildfire burned area caused by climate change and human activity, many previously undisturbed areas will see an increase in post-fire runoff and erosion events. Land managers have considerable interest in mitigating these hydrologic effects both before and after a fire. Physically-based models, like the Water Erosion Prediction Project (WEPP) model, can assist managers in targeting cost effective mitigation strategies. Here, the WEPP model is applied to a catchment in Eastern Arizona which burned in the 2011 Wallow Fire. After calibration, simulations were compared to observed streamflow, peak flow, hillslope erosion rates, and catchment sediment yield for the first five years after the fire. The model performed very well for capturing daily streamflow for the years immediately after the fire (Nash-Sutcliffe Efficiency, NSE, 0.70 – 0.75; r^2, 0.72 – 0.79). Hillslope erosion and sediment yield rates were similarly well captured by the model (NSE, 0.62; r^2, 0.82). After calibration, the model was applied to a nearby watershed without further calibration and described daily streamflow and peak flow with an NSE of 0.57 and r^2 of 0.69. Calibration parameters were generally in agreement with published literature values. The good overall agreement between simulated and observed hillslope erosion rates and sediment yield at the watershed outlet as well as the good agreement in a paired uncalibrated watershed suggests that WEPP is able to capture the hydrologic conditions in the post-fire environment.

Introduction

Wildfire activity in the western US is expected to increase in frequency and extent throughout the 21st century. Many researchers have shown that climate driven factors including earlier snowmelt timing and increased summer drought conditions will extend the typical fire season at both ends (Westerling, et al., 2006; Abatzoglou & Kolden, 2013). These factors are further confounded by large scale increases in fuel loading from legacy management practices and the increased ignitions by human activity in the expanding wildland-urban interface (Nagy, et al., 2018). Besides the direct effects of uninhibited

wildfire, including the loss of life and property, degradation of cultural and recreational sites, and loss of habitat, fire also profoundly impacts hydrological systems.

The relationships between severe fire and elevated catchment runoff and erosion responses is well documented. Critical changes in soil hydraulic properties (SHPs) including hydraulic conductivity, water holding capacity, and bulk density, have been shown to be well correlated to other indicators of fire severity (Moody, et al., 2016). During surface fuel combustion, volatilization and condensation of hydrocarbon compounds often produces a water repellent layer within the top few centimeters of the soil profile (DeBano, 1996; Doerr, et al., 2000). Combustion of soil organic matter during extended smoldering periods as well as the sealing of macropore structures by ash and soil particles contributes to a reduction in water holding capacity of the soil, as well as an increase in the effective bulk density (Giovannini & Lucchesi, 1997; Certini, 2005; Cerdà & Robichaud, 2009). The reduction in surface vegetation and litter also contributes to these changes in hydraulic response through reduced surface roughness, reduced storage, increased raindrop penetration, and reduced evapotranspiration (Fernández & Vega, 2016). Each of these factors contribute to elevated overland flow production from both saturation and infiltration excess processes, a larger water yield, and increased sediment loss.

Post-fire Hydrological Modeling

There is considerable interest between land managers and the research community in developing numerical models to predict post-fire hydrological effects as well as forecast treatment effectiveness (Shakesby, et al., 2016). Many models have consequently been in developed with this intent. Among these, the Water Erosion Prediction Project (WEPP) model is a physically-based hydrology and sediment transport model which has seen wide application in forested and post-fire watersheds. While originally developed for agricultural and rangeland systems, the WEPP model's utility for predicting post-fire hydrological responses has been under constant development over the past decades (Elliot, et al., 2016). Further, many online interfaces for the model have been developed which allow a great amount of accessibility to this otherwise complex model. For example, the Erosion Risk Management Tool (ERMiT, Robichaud, et al., 2007), and Disturbed WEPP (Elliot, 2004) are two interfaces which facilitate post-fire erosion mitigation and management strategy

simulations at the hillslope scale. WEPP can also simulate watershed-scale sediment and hydrological responses through the GIS-based GeoWEPP tool, which allows a user to easily delineate watershed and hillslope boundaries and generate WEPP input files (Renschler, 2003).

Many authors have applied and validated the WEPP model to forested watersheds (Dun, et al., 2009; Brooks, et al., 2016; Srivastava, et al., 2017), however few authors have attempted watershed-scale validation of post-fire runoff and erosion response (Miller, et al., 2011). At the hillslope-scale, ERMiT and Disturbed WEPP, have been validated using hillslope-scale plot studies and suggest that WEPP can provide reasonable post-fire predictions at the hillslope scale (Elliot and Foltz 2001, Larsen and MacDonald 2007, Robichaud, et al. 2016). While these hillslope-scale interfaces have been highly used by post-fire management teams for directing post-fire mitigation practices, there is a great need for watershed-scale scale decision supports to assist in targeting and evaluating effects of post-fire mitigation practices at the watershed outlet. There has never been a full watershed scale assessment of the WEPP model in the post-fire environment.

Objectives

The main goal of this study was to assess the hydrological and sediment response prediction ability of the WEPP model for post-fire catchments. The following outlined objectives were designed in attempt to validate the model for this purpose:

- Apply a modified version of the GeoWEPP model to identify and capture variability in burn severity across topographic gradients at the hillslope scale
- Use observed data to calibrate and assess the ability of the model to simulate watershed-scale, post-fire hydrologic response for catchments within a large wildfire
- Assess the validity of the model by transferring the parameterized model to a nearby catchment with observed flow data.

Site Description

From May 29 to July 8, 2011, the Wallow fire burned through a 217,000-ha portion Eastern Arizona and Western New Mexico starting in the Bear-Wallow Wilderness area (Figure 3.1 and 3.2). We selected two catchments that burned on June 7, 2011, the West Willow Creek (117 ha) and the North Fork Thomas Creek (207 ha) (Figure 3.3), which were subject to previous water yield experiments through the 1980s (Heede, 1987; Gottfried, 1991).

Each catchment supports a first-order ephemeral stream characterized by high flows during spring snowmelt and intense summer storms, however perennial flow begins slightly downstream of the installed weirs (Heede, 1987). The catchments were previously described by a mixed-conifer forest do dominated by quaking aspen (*Populus tremuloides*), Engelmann spruce (*Picea engelmannii*), Douglas-fir (*Pseudotsuga menziesii*), corkbarkfir (*Abies lasiocarpa*), and white fir (*Abies concolor*) (Wagenbrenner 2013). The post-fire plant community is generally comprised of an immediate grass population with a shrub and tree regrowth including New Mexican Locus (*Robinia neomexicana*) and aspen (*P. tremuloides*). Soils are characterized as a rocky, silty clay loam with depths ranging from 500 to 1000 mm (Gottfried, 1983; NRCS, 2017). Heede (1991) further described the underlying bedrock layer as a very porous fractured basalt.

Average annual precipitation ranges from 542 to 1127 mm with approximately half of precipitation occurring as snow. Summer precipitation occurs during the North American monsoon season from July through September with characteristic spatially-limited, high-intensity convective storms. The 10-year return interval 10, 30 and 60-minute rainfall intensities (I_{10}, I_{30}, I_{60}) are 158, 88, and 54 mm hr^{1} while the 2-year return interval intensities for the same durations are 81, 45, and 28 mm hr^{-1} (NOAA, 2017).

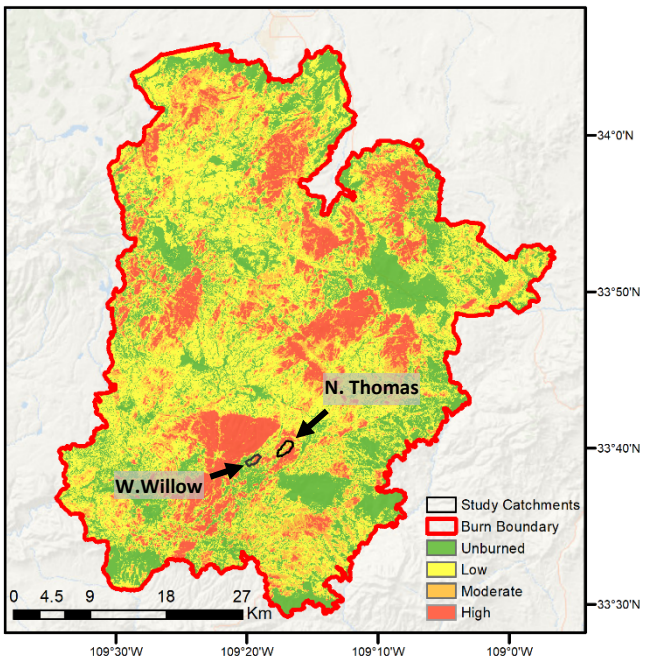

Figure 3.1 Wallow fire burn boundary with West Willow and North Thomas catchments.

Figure 3.2 Location of the Wallow Fire in Eastern Arizona

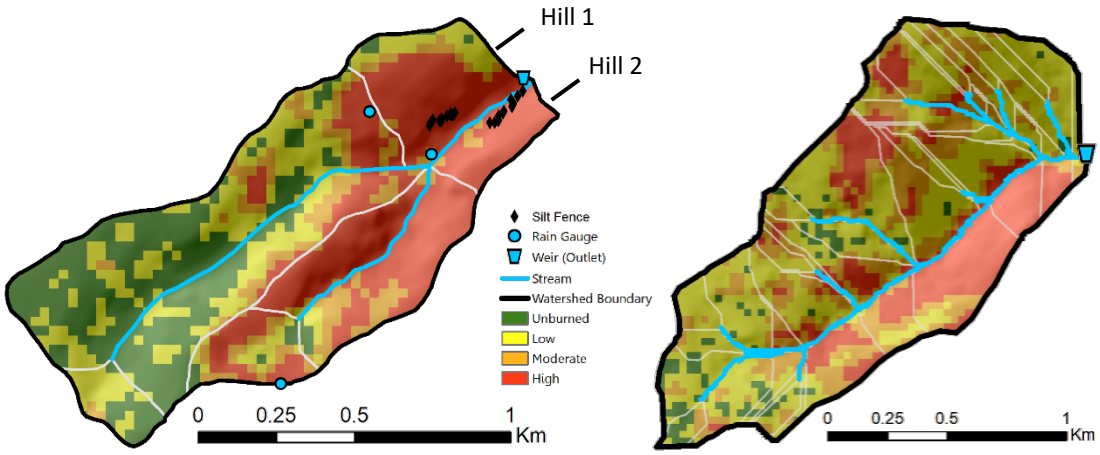

Figure 3.3 a) West Willow and b) North Thomas soil burn severity maps showing silt fence and rain gauge locations. Note Hill 1 and 2, which contain silt fences. Both hillslopes contain a majority high soil burn severity classification.

Field Data

Observed field data were collected from the West Willow catchment for the immediate five-year period following the 2011 Wallow Fire as described by Wagenbrenner (2013). A 120° sharp-crested v-notch weir with two 3 by 6 m concrete settling basins and one natural-ground basin, which were previously installed in 1962, was re-instrumented with an ultrasonic depth sensor and temperature probe (Judd Communications, Holladay, UT) in July 2011. A secondary pressure transducer sensor (CS451, Campbell Science, Logan, UT) was installed in October 2013. 24 trench-bound plots measuring 3 by 30 meters with geo-textile silt fences were established in the high burn severity areas following methods described by Robichaud & Brown (2002) (Figure 3.3a). The weir settling ponds and silt fences were frequently cleaned for the first two years of the study (Figure 3.4). Point-intercept ground cover surveys were conducted using 1-m^2 quadrats along plot transects near each silt fence (Jonasson, 1988). These surveys described the representative percent cover of various categories including vegetation, bare soil, litter, and rocks. A timeline of site visits including sediment and plot cover surveys can be found in Figure 3.4. Four 15.39 cm diameter tipping-bucket rain gauges (HOBO Onset, Bourne, MA) were also placed throughout the catchment with a resolution of 0.254 mm (0.01 in) per tip. Precipitation and streamflow at the North Thomas catchment was similarly monitored with a network of 4 tipping bucket gauges, 120 v-

notch weir, settling ponds, and an ultrasonic sensor, however no silt fences were maintained in this catchment. This data was subject to several quality issues which is discussed later.

A ground corrected soil burn severity map (USDA Forest Service, 2017) was retrieved and examined for accuracy following procedures outlined by Parsons et al. (2010). For the catchments examined in this study, Wagenbrenner (2013) found the map to appropriately represent the immediate post-fire conditions. This map was used to spatially describe vegetation and soil properties as discussed further in the *Modeling Framework* section in Chapter 2.

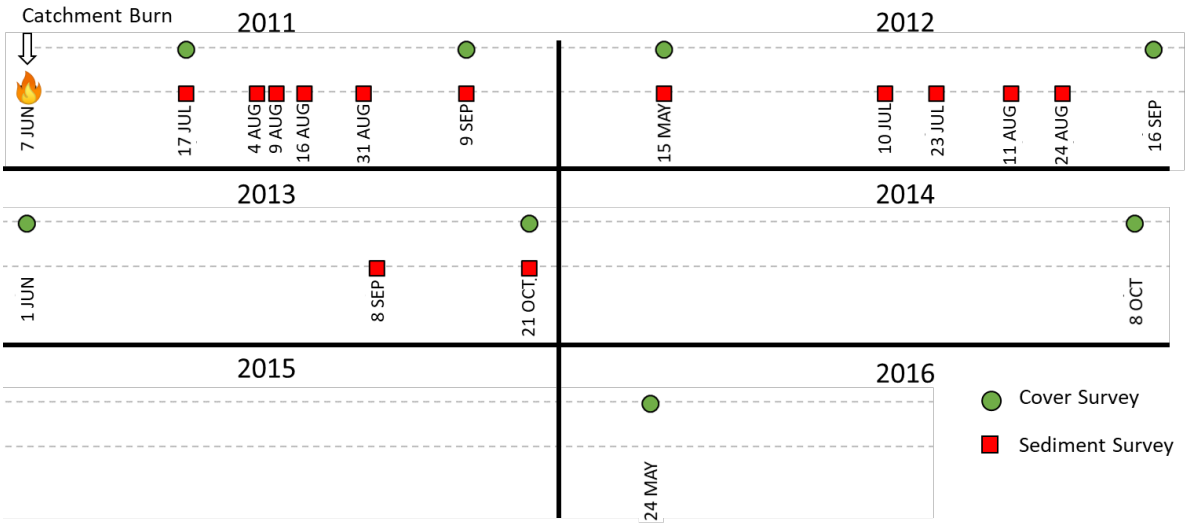

Figure 3.4 Timeline of sediment and plot cover surveys. Red boxes represent sediment surveys and green circles represent cover plot surveys. Some sediment surveys were used solely as reference surveys. The catchment was burned on 7 June 2011.

Methods

Model Description

The WEPP model is a deterministic, process-based sediment transport model which incorporates climatic, topographic, and edaphic data as well as land cover management to estimate soil loss, erosion, and hydrology at the hillslope scale (Flanagan & Nearing, 1995). Within the default model framework, representative rectangular hydraulic response units can be connected in a channel structure to allow for watershed-scale processing and simulation (Wang, et al., 2010). Hillslope processes include infiltration, surface runoff, lateral subsurface flow, soil detachment, transport, and deposition, as well as rudimentary vegetation regrowth.

Model inputs including soil, vegetation, slope, and climate, can be further assigned at the sub-hillslope scale using built-in overland flow elements (OFEs, Figure 3.5). This functionality allows multiple inputs to be assigned to a single hillslope as well as provides a better representation of hillslope runoff partitioning by enabling the model to calculate hydrology at this smaller scale (Boll, et al., 2015).

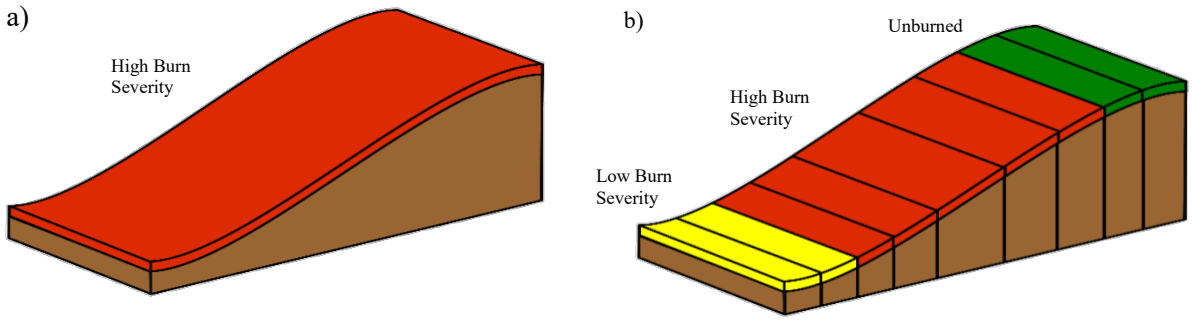

Figure 3.5 a) Example of a representative WEPP hillslope showing a default single-OFE hillslope with a single burn severity and b) custom OFE method where multiple OFEs are used to represent within-hillslope heterogeneity

Due to the rectangular hillslope abstraction, all hillslope and OFE processing in WEPP is calculated by unit width (Flanagan & Nearing, 1995). This restricts the model from incorporating lateral planform curvature, forcing sediment loss, deposition, and yield to be described by distance from the hillslope bottom. Consequently, all model estimates are given per unit width at varying distances along the slope profile.

A modified version of WEPP was used which includes routines for streamflow post-processing from deep percolation through a linear reservoir as described by Brooks, et al. (2016) and Srivastava, et al. (2017). This framework allows the model to capture flow which falls below the modeled domain of individual hillslopes, but which is assumed to be released back into the watershed streamflow.

Topographic Characterization

Model inputs were generated using the TOPAZ model within the GeoWEPP framework (Renschler, 2003). This framework generates a network of representative rectangular hillslopes with characteristic slope profiles connected by stream channels where soil and vegetation properties are assigned based on the simple majority present in the hillslope area (Figure 3.5b). To simulate the effects of within-hillslope hydraulic connectivity of discrete burn severity patches, we developed automated procedures to define hillslope

OFEs. Each hillslope was segmented into 9 unique OFEs based on the Topographic Position Index (TPI 300) calculated with a 10m DEM (Weiss, 2001). The TPI of a cell is a unitless value which describes the relative position along a slope, where positive values represent a ridge top and negative values represent a valley floor. Conceptually, this method allows the model to represent multiple burn severity classes in a hillslope, rather than a single soil and vegetation type assigned to the entire hillslope based the largest fraction of the delineated hillslope area. For example, where there are low severity and unburned patches in the hillslope which are are described by multiple OFEs, which would otherwise not be represented (Figure3.6b). For this procedure, we used a 10 m DEM from the National Elevation Dataset (USGS, 2015). Burn severity classes were assigned to each OFE based on the majority severity class occupying the each TPI band. This classification of unburned, low, moderate, or high severity was used to assign soil and vegetation files to the OFE.

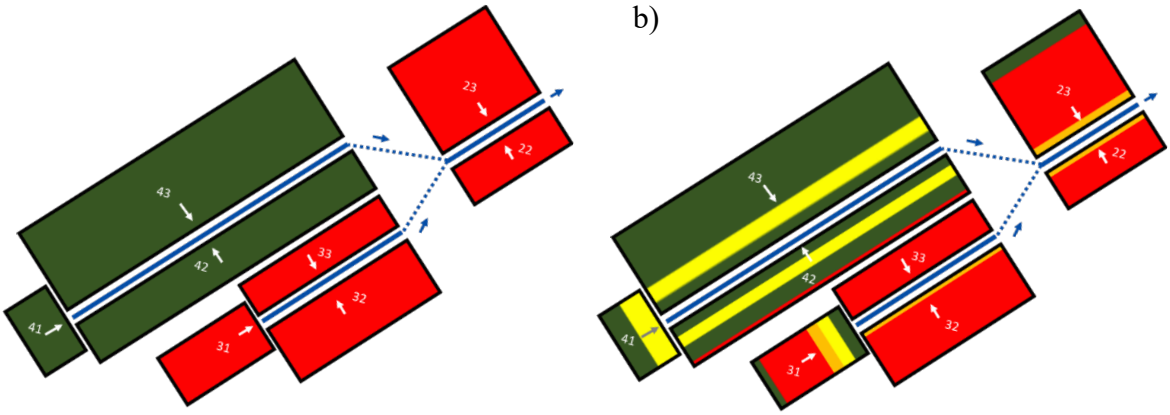

Figure 3.6 WEPP rectangular hillslope representations for the West Willow catchment showing classified burn severity for a) the default GeoWEPP delineation method with a single OFE per hillslope and b) the multiple OFE method based on the TPI 300. Numbers signify WEPP identification codes

Data Sources

A suite of remotely sensed and modeled data were required to generate or initialize the model input files before calibration. This includes properties of soil, spatial vegetative recovery, and weather attributes including solar radiation, dew point, and wind speed.

Vegetation – A series of Landsat 7 ETM+ (USGS, 2017) NDVI images were used to spatially extrapolate observed vegetative cover parameters over the catchment. Each scene was selected corresponding to plot cover observation dates and screened for cloud and smoke

percentage less than 5% of the study area. Observed canopy cover values for each plot survey date were calculated as a percentage of area covered by green vegetation (grass, forb, shrub) and were averaged by corresponding 30 x 30 m Landsat pixel. A linear regression between the corresponding NDVI scene pixel and plot canopy cover observation was fit to the data for the July – October study period where a total of 9 pixels for each scene represented the 24 plot observations. A total of 9 Landsat scenes were used in this regression yielding 81 distinct pixel-observation pairs. This procedure was based on methods described by Soudani, et al. (2012) who noted similar correlations between NDVI and foliar canopy cover.

Soil – Regional soil properties were retrieved from the STATSGO2 dataset (NRCS, 2017) and a baseline soil file was generated for this soil type which described unburned conditions. Additional field observations by Heede (1987) and Wagenbrenner (2013) including sand, silt, clay, and rock composition were used to generate this file. Soil files describing unburned, low, moderate, and high burn severity soil properties were initialized prior to calibration with changes to saturated hydraulic conductivity (Fox & Carrega, 2007; Moody & Ebel, 2014), bulk density (Giovannini & Lucchesi, 1997; Fox & Carrega, 2007), water content at field capacity and wilting point (Ebel, 2012), organic matter, and rill and interrill erosivity (Covert & Robichaud, 2005, Robichaud, et al., 2007). These properties were generally modified using parameter ranges suggested by observations described in the literature for similar textural classifications and were used later to guide calibration.

Weather – A single weather file was produced for the watershed using the median observed breakpoint precipitation from the network of precipitation gauges within each watershed. Observed daily maximum and minimum temperature was measured from the ultrasonic stage height sensor. Solar radiation was calculated using the difference between minimum and maximum daily air temperature described by Bristow and Campbell (1984) with modifications to allow for seasonal variation as noted by Ndlovu (1994). Daily dew point was similarly modeled using an empirical regression described by Kimball, et al. (1997). See Appendix A for references to these methods. Wind speed and direction values were gathered from the nearest weather station which recorded these values in Alpine, AZ (33°50' N 109°09' W).

Model Calibration

The following statistics were used to quantify agreement between model predictions and observations and guide calibration. Pearson's *r* , the coefficient of determination, r^2, and the Nash-Sutcliffe Efficiency (NSE) statistic were used to describe model fit to observations. Both Pearson's *r* and r^2 describes the proportion of observed dispersion is explained by a model. The values of *r* range from 1 to -1, where a value close to ±1.0 indicates the observed and simulated values are well correlated with each other. r^2 ranges from 0 to 1, where a value near 1.0 indicates the model is capturing a higher proportion of observed variability. These statistics may suggest good agreement even in the case of systematic over-under prediction (Krause, et al., 2005). For this study, both values are represented for simple linear regressions. The Nash-Sutcliffe Efficiency (NSE) statistic is commonly used to assess the fit of a hydrological model to observed values (Nash & Sutcliffe, 1970). The statistic has an upper bound of 1.0 which indicated perfect agreement between observed and predicted values. Values of 0.7 to 0.9 are common for well-calibrated models whereas values below 0.4 may indicate a model is capturing basic hydrological mechanisms (Foglia, et al., 2009). Values below 0.2 are likely insufficient for most applications. Lastly, the standard error (SE) was used to represent the amount of variation was found between observed and simulated sets.

$$r = \frac{\sum_{i=1}^{n}(x_i-\bar{x})(y_i-\bar{y})}{\sqrt{\sum_{i=1}^{n}(x_i-\bar{x})}\sqrt{\sum_{i=1}^{n}(y_i-\bar{y})}} \tag{3.1}$$

$$NSE = 1 - \frac{\sum_{i=1}^{n}(x_i-y_i)^2}{\sum_{i=1}^{n}(x_i-\bar{x})^2} \tag{3.2}$$

$$SE = \frac{\sqrt{\frac{1}{n}\sum_{i=1}^{n}(x_i-\bar{x})}}{\sqrt{n}} \tag{3.3}$$

where n is total number of data points, x_i is the observed value at time i, y_i is the predicted value at time i, $\bar{x}$ is the average of observed values for the study period, and $\bar{y}$ is the average of predicted values for the study period as:

$$\bar{x} = \frac{1}{n}\sum_{i=1}^{n} x_i \; ; \; \bar{y} = \frac{1}{n}\sum_{i=1}^{n} y_i \tag{3.4}$$

In this study we followed a manual sequential parameterization and calibration approach for vegetation and soil parameters in the West Willow catchment. The following

section describes the calibration procedure used in this study for capturing the post-fire vegetative and hydrologic recovery.

Vegetation Recovery – The NDVI-canopy cover relation was used to fix initial condition and vegetation regrowth parameters were fixed to fit canopy cover using default WEPP plant growth routines. The following parameters to match this post-fire vegetative regrowth: initial canopy, rill and interrill cover, maximum leaf area, energy to biomass ratio, growing degree days to emergence, radiation extinction coefficient, maximum canopy height, percent of canopy that senesces, date to senescence, and an empirical canopy cover coefficient. The r^2 value between modeled and estimated canopy cover for each burn severity class was used to manually guide calibration. Parameters were adjusted incrementally, one-at-a-time, between simulations. Each parameter was adjusted multiple times throughout this procedure, and the order of parameter calibration was influenced *ad hoc*.

Soil Recovery – After initial assignment, soil properties were calibrated separately for each year with an iterative, semi-automated, stepwise approach using the NSE and r^2 values for daily average streamflow and peak flow as guiding metrics. An automated script was developed which completed bulk simulations where single calibration parameters were varied over a predefined parameter range. Based on existing literature it was assumed that wildfire could affect the bulk density, hydraulic conductivity, and water content at field capacity and wilting point for the top 200 mm of the soil horizon. These parameters were then set based on the overall agreement between simulated and observed daily streamflow and peak flow based on NSE and r^2 statistics.

Runoff and Baseflow – The linear reservoir baseflow recession coefficient, k_b, was calibrated with falling limbs of a subset of pre- and post-fire hydrographs as suggested by Beck, et al. (2013). The deep seepage loss coefficient, k_s, was used as a calibration parameter to simulate losses to deep groundwater. k_b was calculated from daily flow Q (mm day^{-1}) at time t as:

$$k_b = -\ln \frac{Q_t}{Q_{t-1}} \tag{3.5}$$

Erosion – After vegetative and hydrologic property calibration, erodibility parameters including critical shear stress, rill erodibility, and interrill erodibility, were calibrated using hillslope sediment loss and watershed sediment yield. Channel soil properties were used to

further calibrate watershed sediment yield by adjusting critical shear stress, erodibility, and Manning's roughness.

Model Evaluation

Overall model performance was evaluated on the ability to describe daily streamflow, peak streamflow, and event-based sediment delivery at the hillslope and watershed scales for the North American seasonal monsoon season (July – October). For the West Willow catchment, this was examined for the first five years after the fire. For the North Thomas catchment, data quality issues restricted validation to only the fire year. All statistical calculations were performed using the R statistical package.

Streamflow – A comparison of observed and modeled streamflow for daily average flow and daily peak flows were used to assess the model's ability to capture the watershed hydrological response. The NSE and r^2 values were calculated for each year. For both metrics, a threshold value of 0.4 or greater was used to determine an adequate fit of the model in this application as suggested by Foglia, et al., (2009).

Sediment – Geotextile silt fence-based sediment observations from two high-burn severity hillslopes (Hill 1 and 2, Figure 3.3a) were compared to modeled sediment transport rates at corresponding locations on both representative hillslopes. Daily modeled sediment loss rates at these locations were summed for each silt fence cleanout period to produce a single estimate for each hill. The simulated value was then compared to the observed average value for each hillslope and assessed using the r^2 statistic. Sediment collected between years was assumed to be generated from the previous summer as suggested by Wagenbrenner (2013). Watershed sediment simulations were similarly compared to event-based settling pond cleanout periods. The ponds were assumed to have captured all exiting bedload sediment but not the suspended fraction. Following the review of sediment fractionation by Turowski, et al. (2010) as well as sparse suspended sediment samples and anecdotal results from similar studies (Wagenbrenner, personal communication, 2018), the suspended fraction was estimated at 50%. This was held constant for the study period.

Uncalibrated Assessment

The methods described above for topographic delineation, input assignment, breakpoint weather file generation, and streamflow evaluation were repeated for the North Thomas catchment. For this validation component, soil and vegetation properties which were described for the West Willow catchment were simply reassigned based on topography and burn severity without further calibration. The uncalibrated daily average and peak flows for this catchment were compared to observed as described above. Due to data quality issues, this validation effort was only conducted for the fire year summer monsoon season.

Results

Vegetation Recovery

Immediately after the fire, high burn severity plots were characterized by 80 – 100% exposed mineral soil. Some grass establishment was observed in the high burn severity plots within three months of the catchment burn date. The observed vegetative cover for these plots followed a seasonally oscillating vegetation recovery trend with peak pre-senescence vegetative cover generally higher than the beginning of the growing season. Within four years post-fire, the mineral fraction of cover was reduced to below 20% in the high severity plots. NDVI correlated well with plot-observed canopy cover using a simple least squares regression (Pearson $r \sim 0.81$; $p < 0.001$) for the high severity plots throughout the observation period. For each discrete hillslope OFE, the regression equation:

$$Canopy\ Cover = 1.854 * NDVI - 0.328 \tag{3.6}$$

was used to produce spatiotemporal canopy cover series (Figure 3.7). This series shows the high burn severity areas showed minimal vegetative cover within the first two years with values ranging from 35 – 68% lower than in unburned areas, while percent cover was within 25% of unburned areas by 2013. Average low burn severity TPI bands showed an increase of 15 – 18% within three months of the catchment burn, after an 18% decrease in canopy cover compared to unburned areas immediately after the fire.

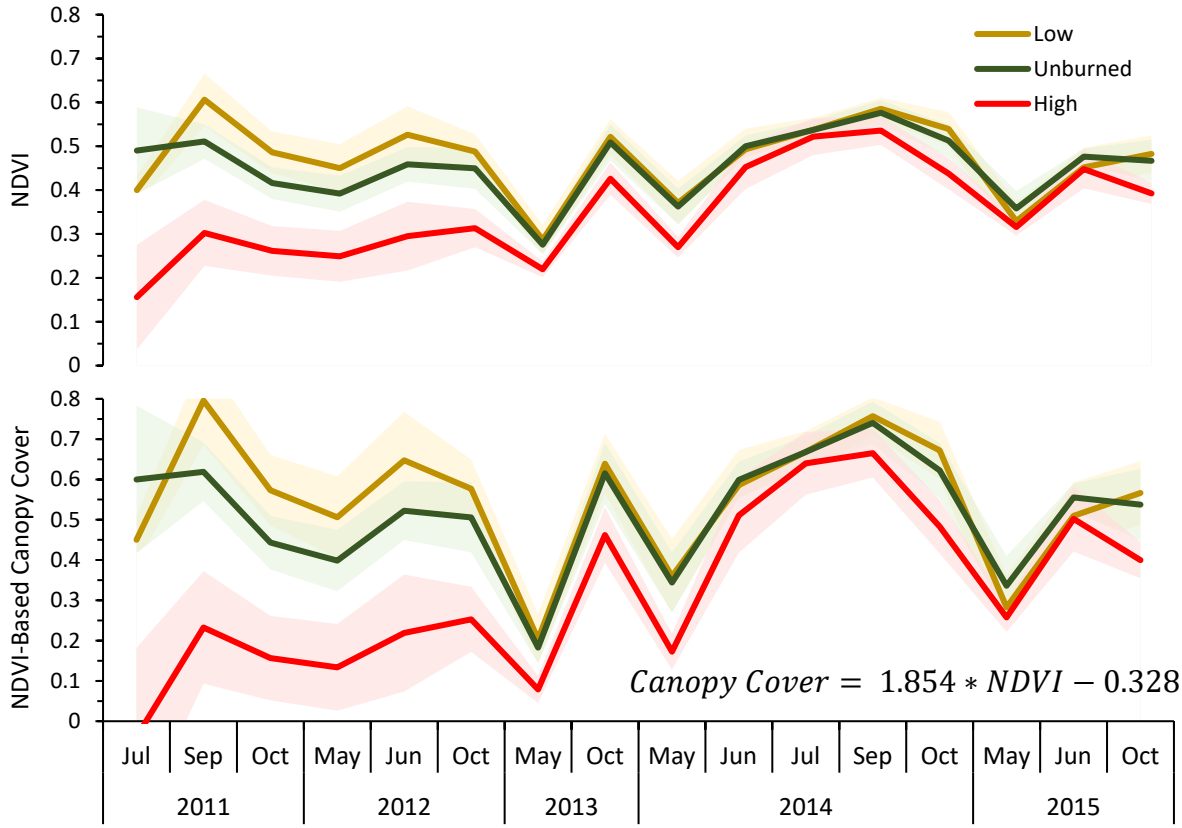

Figure 3.7 a) Landsat NDVI values and b) estimated canopy cover derived from NDVI for TPI bands represented as Unburned, Low, and High burn severity. No locations were classified as Moderate burn severity. Each series represents the average of each respective-burn severity class while envelopes show standard deviation. Simple linear regression equation is also shown. Note irregular temporal scale due to Landsat scene selections.

The observed and modeled canopy cover recovery trends were used to manually calibrate the WEPP regrowth and initial condition parameters for each burn severity class. This parameter calibration was generally informed by the range of values described in the literature (Srivastava, et al., 2018, *in press*). All parameters used for calibration can be found in Table 3.1 and 3.2.

The WEPP modeled canopy cover for the high burn severity class closely matches both observed and remotely sensed canopy cover values using a simple least squares regression (pearson $r = 0.83$, $p < 0.0001$, $n = 27$) (Figure 3.8).

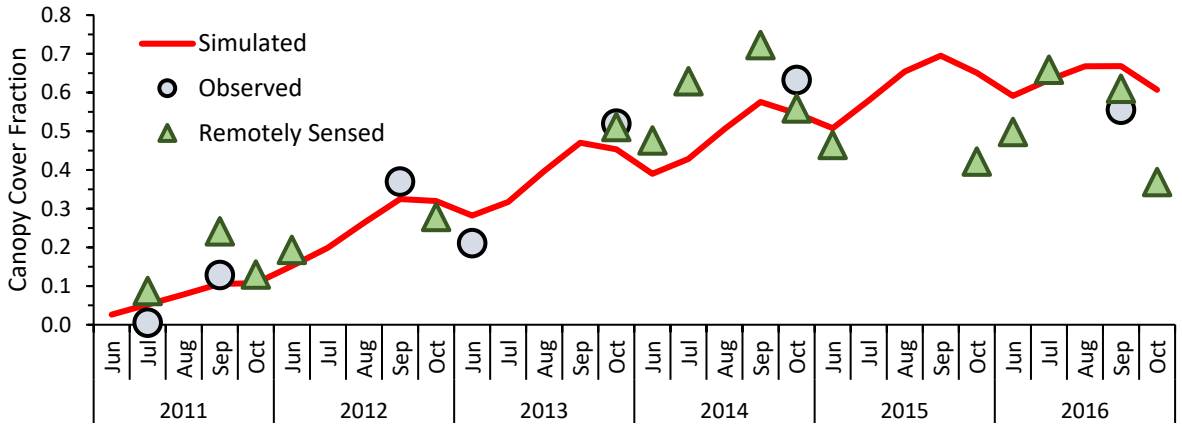

Figure 3.8 Observed canopy cover measurements from the high severity ground plots and corresponding NDVI-based canopy cover compared to simulated canopy cover regrowth. Remotely sensed canopy cover was averaged for all 9 pixels corresponding with a plot for available dates. Values are shown from June to October.

Table 3.1 WEPP plant growth parameters for each burn severity class. Only parameters significant to vegetative cover or sensitive for vegetative recovery are shown. Percentages are shown as decimal values.

Plant Growth and Harvest Parameters	Unit	Unburned	Low	High
Biomass energy ratio	kg MJ^{-1}	2.5	2.0	1.8
Height of post-harvest standing residue	m	0.3	0.3	0.3
Plant stem diameter at maturity	m	0.5	0.05	0.005
Growing degree days to emergence	-	10	10	90
Growing degree days for growing season	-	80	80	150
Canopy, LAI and Root Parameters				
Canopy cover coefficient	-	13	10	8
Maximum canopy height	m	10	10	0.2
Maximum leaf area index	-	9	3	2
Senescence Parameters				
Percent canopy remaining after senescence	%	0.8	0.6	0.5
Percent of growing season when LAI declines	%	0.5	0.5	0.2
Percent of biomass remaining after senescence	%	0.8	0.8	0.6
Period over which senescence occurs	-	120	120	90
Residue Parameters				
Decomposition constant (below ground)	-	0.002	0.002	0.004

Table 3.2 Initial WEPP plant conditions for each burn severity class. Percentages are shown as decimal values.

Ground and Canopy Cover	Unit	Unburned	Low	Mod	High
Initial canopy cover	%	0.6	0.4	0.1	0.0
Initial rill cover	%	0.5	0.5	0.05	0.0
Initial interrill cover	%	0.5	0.5	0.05	0.0
Initial total dead root mass	kg m^{-2}	0.2	0.2	0.2	0.2
Initial total submerged residue mass	kg m^{-2}	0.2	0.2	0.2	0.2

Soil Recovery

Soil properties for the top 200 mm of soil were calibrated each year for low, moderate, and high soil burn severity classes (Table 3.3). Soil bulk density for the fire year ranged between 1.6 and 1.9 g cm^{-3}. The bulk density decreased over the study period to 1.6 g cm^{-3} for all burn severity classes. Saturated hydraulic conductivity in high burn severity soils was set to 0.1 mm hr^{-1} for the fire year post-fire and was increased through calibration for the next two years. The calibrated values for water content at field capacity and permanent wilting point for high burn severity soils started at 10% and 5% respectively before returning to near pre-fire values by 2015. Interrill erodibility values were kept constant between years and ranged between 500,000 to 5,000,000 kg s m^{-4} from low to high severity. Rill erodibility was set at 0.0006 s m^{-1} for the first year in the high burn severity soils and was lowered to 0.0003 s m^{-1} for the following years. This parameter was held at 0.0002 s m^{-1} for low and moderate burn severity soils and 0.0001 s m^{-1} for the unburned soils.

All soils were described as a rocky, silty clay loam with sand content between 20 and 30%, clay content between 30 and 40 %, and gravel content between 30 and 35% (Table 3.4). All soil properties below 200 mm were assumed to be unaffected by wildfire and therefore remained constant throughout the simulation and across the watershed. For the top 200 mm layer, particle size composition was also held constant throughout the simulation. Bedrock hydraulic conductivity was set to 10 mm hr^{-1} to describe a fractured basaltic layer.

Table 3.3 Calibrated soil properties by year and severity class describing the top 200 mm of the soil profile. The unburned soil class calibration did not change between years.

	Bulk Density	Hydraulic Conductivity	Aniso-trophy.	Field Capacity	Wilting Point	Organic Matter	Interrill Erodibility	Rill Erodibility
	g cm^{-3}	mm hr^{-1}	-	m^3 m^{-3}	m^3 m^{-3}	%	kg s m^{-4} x1000	s m^{-1}
Unburned								
	1.5	100	10	0.2	0.1	7	100	0.0001
Low								
2011	1.6	10	50	0.15	0.1	2	500	0.0002
2012	1.6	15	50	0.15	0.1	2	500	0.0002
2013	1.6	20	50	0.15	0.1	2	500	0.0002
2014	1.6	30	10	0.15	0.1	2	500	0.0002
2015	1.6	80	10	0.15	0.1	2	500	0.0002
Moderate								
2011	1.7	1	50	0.12	0.1	1	5000	0.0002
2012	1.7	2	50	0.12	0.1	1	5000	0.0002
2013	1.7	2	50	0.12	0.1	1	5000	0.0002
2014	1.6	20	10	0.15	0.1	1	5000	0.0002
2015	1.6	60	10	0.15	0.1	1	5000	0.0002
High								
2011	1.9	0.1	50	0.1	0.05	0.5	5000	0.0006
2012	1.9	0.5	50	0.1	0.05	0.5	5000	0.0003
2013	1.8	2	50	0.12	0.05	0.5	5000	0.0003
2014	1.8	10	10	0.12	0.08	0.5	5000	0.0003
2015	1.6	50	10	0.15	0.1	0.5	5000	0.0003

Table 3.4 General soil properties retrieved from the STATSGO2 database and modified based on field observations. Apart from the Layer 1 properties described in Table , these were held constant for each severity class and year. Bedrock layer thickness is also shown.

	Depth	Bulk Density	Hydr. Cond.	Field Capacity	Wilting Point	Sand	Clay	Rock
	mm	g cm^{-3}	mm hr^{-1}	m^3 m^{-3}	m^3 m^{-3}	%	%	%
Layer 1	200	- See Table -				20	30	30
Layer 2	300	1.3	100	0.15	0.05	30	30	30
Layer 3	500	1.3	100	0.10	0.05	20	40	35
Bedrock	>500	-	10	-	-	-	-	-

Channel Properties

The West Willow catchment was modeled with a 3-channel network with two first order segments and one second order segment. Critical shear stress and Manning's *n* were

used to calibrate watershed sediment yield and were set to 9 N m^{-2} and 0.1 respectively. This was done after calibration of hillslope sediment. Manual adjustments were made to these properties *ad hoc*.

Hydrologic Response

Daily Flow

The baseflow recession coefficient, k_b, was calculated from approximately 20 historical and recent flow recession observations and ranged from 0.12 to 0.17. A median value of 0.15 day^{-1} was selected to represent the catchment. The deep seepage coefficient, k_s, was adjusted throughout the calibration period and set at 0.05 day^{-1}. These appear to appropriately match the majority of streamflow recession curves for all years within the study period and were held constant between years.

During the 2011 summer monsoon period and immediately after the fire, the modeled daily average flow matched the uncharacteristic 'flashy' nature of the observed hydrograph. This resulted in a total of 11 large peaks in the daily average flow. The two largest peaks in daily average flow during this period were on 3 and 10 Aug with an observed flow of 2.2 and 2.5 mm day^{-1} respectively. The model was able to accurately describe both peaks with predicted values of 2.63 and 2.5 mm day^{-1} respectively. The third largest peak during the 2011 period was on 3 Oct. at 2.05 mm day^{-1}, however the model underpredicted flow on this date. In all cases, the peak daily average flows were accurately described and the NSE value for this period was 0.70. Similar peaks in daily average flow were observed during the 2012 monsoon season, however there were only three major peaks on 8 Aug., 20 Aug., and 23 Aug. 2012. The model was similarly able to capture these peaks however the modeled baseflow recession during this period appears to lag the observed recession. The NSE value for this period was 0.75. The following three study periods for 2013, 2014, 2015 were all characterized by a much less 'flashy' daily average water yield. In these cases, the model slightly underpredicted the peaks in daily average flow, however the modeled baseflow recession appropriately matches observations. For these years, the NSE value was 0.71, 0.58, and 0.61 respectively(Figure3.9).

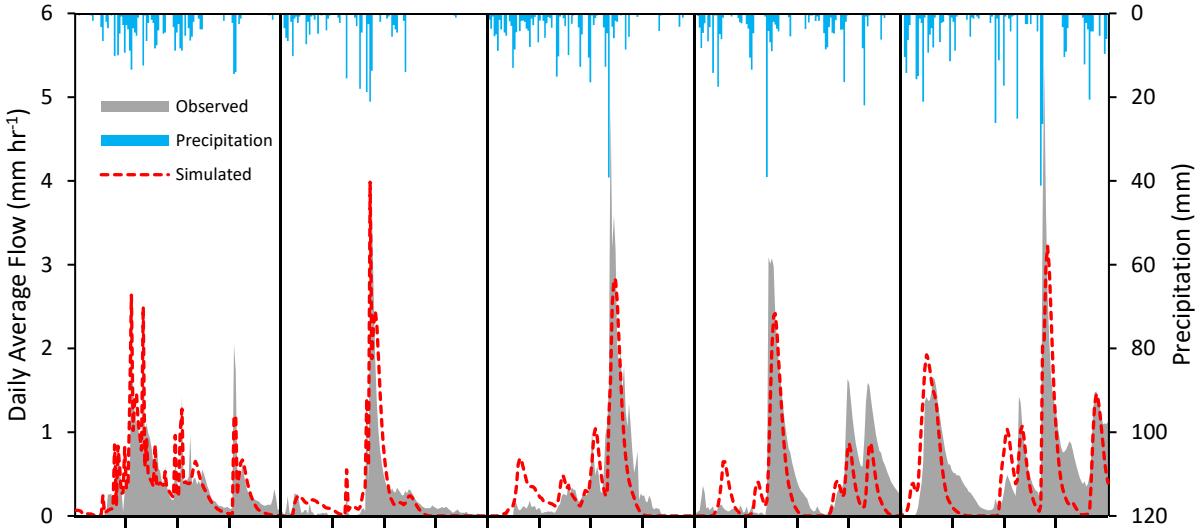

	2011	2012	2013	2014	2015
NSE	0.70	0.75	0.71	0.58	0.61
r^2	0.73	0.79	0.72	0.68	0.65
SE	0.24	0.25	0.40	0.39	0.46

Figure 3.9 Simulated and observed daily average streamflow for the West Willow catchment for the summer monsoon period (July – October). Nash-Sutcliffe Efficiency, r^2 and standard error for each year are shown. The NSE for the collective simulation period was 0.70.

Peak Flow

During the 2011 study period (11 Jul. – 31 Oct.), a total of 24 runoff events greater than 1 mm day^{-1} were observed compared to 15 runoff events which were simulated. The model tended to underpredict peak flow during this period. Five events were observed with a 30-minute rainfall intensity greater than 10 mm hr^{-1}. The NSE and r^2 values for this period were 0.30 and 0.60 respectively. Points below the one-to-one line represent an underpredicted value (Figure 3.10). In 2012, 8 runoff events were observed compared to 7 which were simulated. The maximum simulated peak flow during this summer period was 71.8 mm day^{-1} compared to the observed 74.1 mm day^{-1} (Figure 3.10). The NSE and r^2 values for this period were 0.74 and 0.78. Similar to the apparent recovery seen in the daily average flow, peak flows for the 2013 period were an order of magnitude lower than the previous two years with a maximum observed peak of 7.1 mm day^{-1}. For this event, the modeled peak flow was 8.8

mm day^{-1}. The NSE and r^2 values for this period were 0.38 and 0.87 respectively. For the remaining years, very few runoff events greater than 1 mm day^{-1} were recorded or simulated.

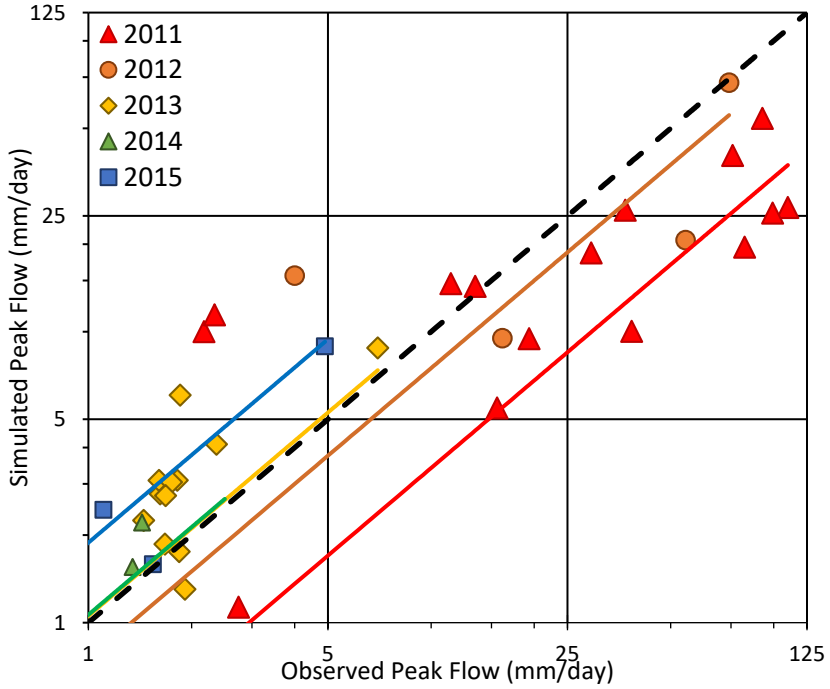

Figure 3.10 Observed and simulated peak flows above 1 mm day^{-1} for the West Willow catchment by year. Trend lines represent a linear least squares fit with a zero intercept. The extent of each line shows the relative maximum magnitudes of the values. Dashed line shows 1:1. Note log scale.

Sediment Response

Watershed Sediment

Between 2011 and 2012, the weir settling ponds were surveyed for sediment volumes on eight occasions (Figure 3.11 and 3.12). Six of these collection periods were in 2011, which resulted in a total of 2.43 Mg ha^{-1} of observed total sediment. The maximum observed value for a single collection period was 0.81 Mg ha^{-1} from 3 Aug. to 10 Aug., a total of 7 days. In 2012, only two collection periods were conducted with a total of 0.47 Mg ha^{-1} observed for this year. The model accurately predicted watershed sediment for both years with a NSE value of 0.62, r^2 of 0.82 and standard error of 0.10. For the first collection period, the model overpredicted sediment yield by 37%, however most other periods did not exceed a ± 10% over/under prediction.

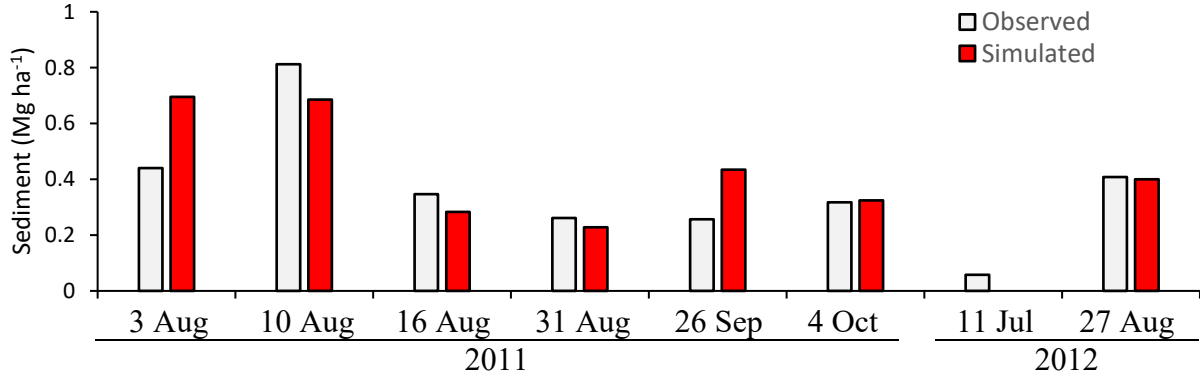

Figure 3.11 Observed and simulated watershed sediment for each collection date. Simulated values were summed for the duration of the collection period.

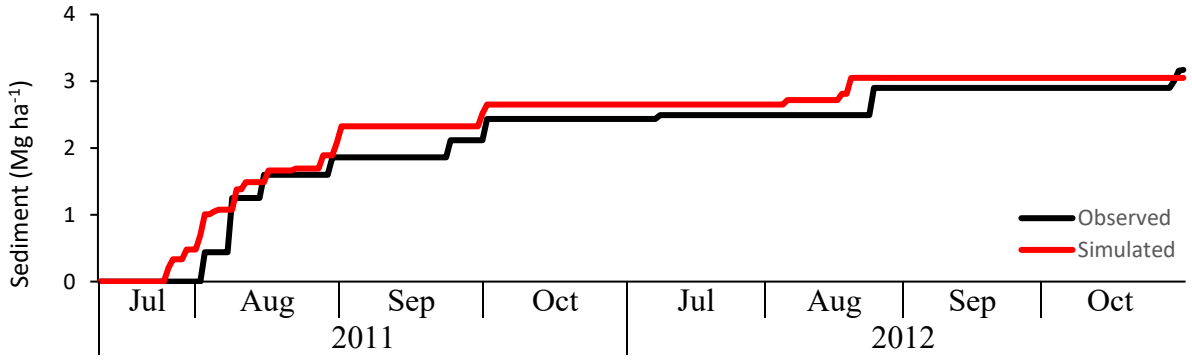

Figure 3.12 Cumulative watershed sediment estimates and observations for the first two years after the fire.

Hillslope Sediment

Hillslope erosion rates were observed for hill 1 and 2 (see Figure 3.3 for location) for the first two years after the fire (Figure 3.13). For this analysis, observed values were averaged by hillslope for each silt fence cleanout period. Almost half of the observed sediment loss was produced within the first collection period on August 3rd with an average rate of 57.6 Mg ha^{-1}. The main differences in erosion rate between hill 1 and 2 is seen during this period, where Hill 1 saw an average erosion rate of 70.3 Mg ha^{-1} while hill 2 showed an average loss of 44.9 Mg ha^{-1} of the total sediment observed. The following five cleanout periods in 2011 consequently produced approximately 30% of total observed sediment loss for the two years. Finally, the four collection periods in 2012 produced approximately 10% of the total loss.

The model simulations of hillslope erosion rates for both hillslopes were well correlated with observed rates with an r^2 value of 0.73 for the all collection periods. The first collection period estimate was much lower than the observed value but was still within the second quartile of the observed range. During 2011, the model overpredicted two other collection periods, 15 Aug. and 26 Sep., by more than double. Following the observed differences between hill 1 and 2 with west and east aspects respectively, the model was able to correctly differentiate between the magnitudes of both hillslopes (Figure 3.14).

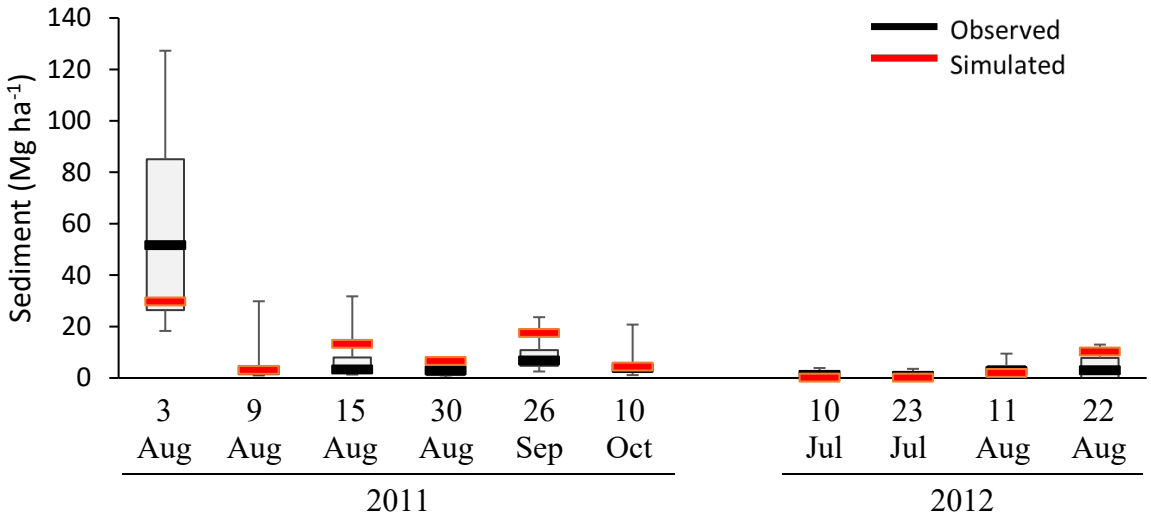

Figure 3.13 Median sediment loss from observed plots (n=24) compared to simulated yield for the same collection period for 2011 and 2012. Boxes represent 1st and 3rd quartiles; whiskers represent min. and max. observed values. Simulated yield for each period is shown in red.

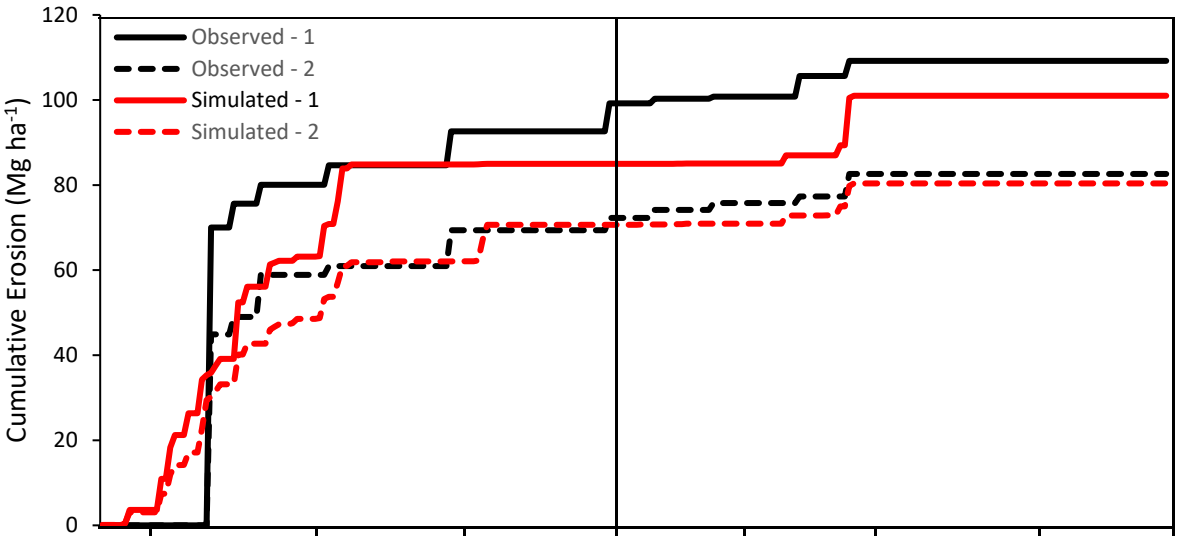

	2011	2012
NSE	0.71	0.72
r^2	0.70	0.95
r	0.84	0.97

Figure 3.14 Cumulative observed (black) and modeled (red) hillslope erosion rates shown for two hillslopes with opposing aspects; Hill 1 (west, solid) and Hill 2 (east, dashed).

North Thomas Validation

The hydrologic response of the North Thomas catchment described by observed peak and daily average flow values were similar to that of the West Willow catchment (Figure3.15). A similar 'flashy' hydrograph for the 2011 period shows the peaks in daily average flow ranged from 3 to 9 mm day^{-1}. The largest peak flow was observed on 7 Sep. with a value of 101.3 mm day^{-1}. After applying the model to the North Thomas catchment using the same soil and vegetation parameters as the West Willow catchment, the model fit well to observations for both metrics. During the 2011 period, this resulted in a NSE value of 0.57, and an r^2 value of 0.69 for daily average flow (Figure 3.15). The observed peaks in daily average flow were consistently larger than the modeled peaks, by approximately 50 – 100%. Baseflow recession appears to be well represented by the model for the majority of events, with the exception of the late October period. Unlike the simulations for the West Willow catchment, peak flows were overestimated by an average of 38% however the model was well

fit to the data with an r^2 of 0.73 (Figure3.16). The simulated value for the maximum peak flow on 7 Sep. was 138.3 mm day^{-1} compared to the observed 101.3 mm day^{-1}.

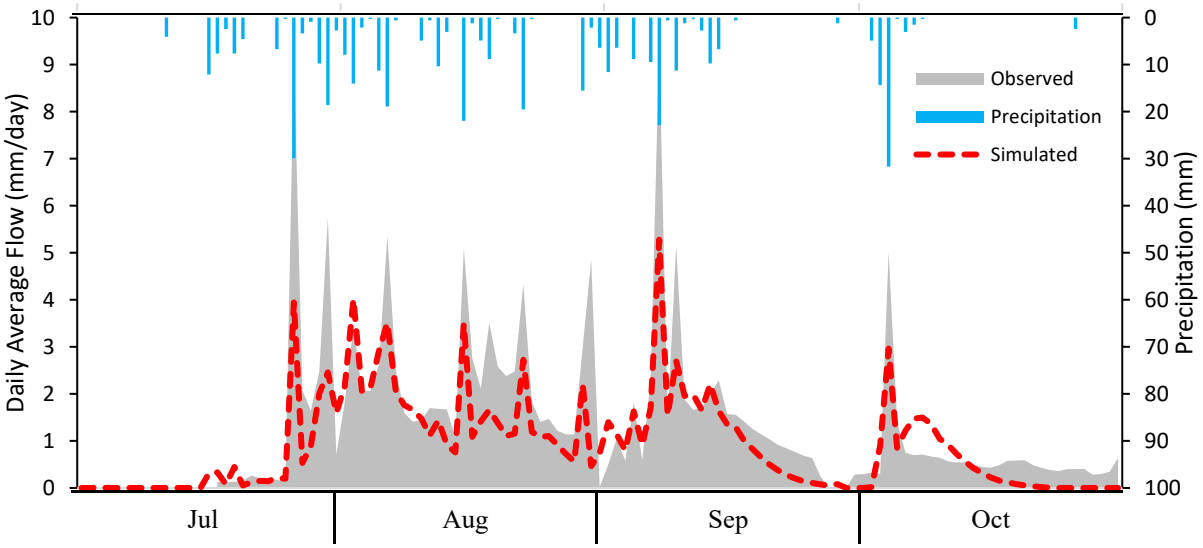

	2011
NSE	0.57
r^2	0.69
r	0.83
SE	0.95

Figure 3.15 Uncalibrated simulated and observed daily average flow for the North Thomas catchment during the 2011 observation period.

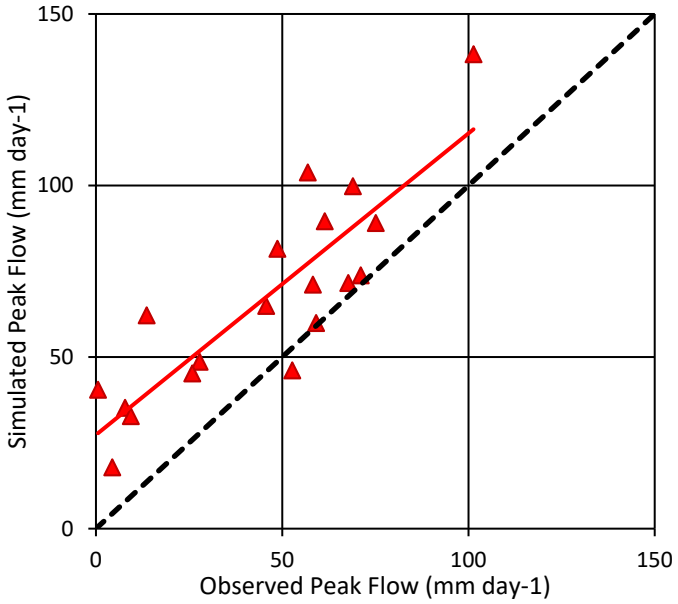

Figure 3.16 Uncalibrated simulated and observed daily peak flows for the North Thomas catchment for the 2011 observation period. Dashed line shows 1:1. $r^2 = 0.73$, $r = 0.85$

Discussion

Overall, the model performed very well during calibration for the West Willow catchment. The main metrics used during model calibration were largely focused on simulated fit to daily average and peak flows. The daily average flow NSE value of 0.67 for the entire study period suggests a good fit for daily flow. The two years immediately after fire, 2011 and 2012, saw the largest hydrologic impact as indicated by the relatively extreme peak flows compared to the later years. For these two years, the daily average flow NSE values were 0.70 and 0.75, indicating the model performed better or was possibly better calibrated for the immediate post-fire effects. By looking at peak flows however, the model generally underpredicted values for 2011 compared to 2012. For these periods, the NSE and r^2 values for peak flows were 0.30 and 0.60 for 2011 and 0.74 and 0.78 for 2012.

The model slightly underpredicted the first major observed hillslope sediment production period, however the later estimates are well fit to observed ranges. Larsen and MacDonald (2007) documented similar trends when applying the WEPP model to a post-fire watershed in Colorado. In this study, the authors suggested a threshold of 1 Mg ha^{-1} yr^{-1} over which events would tend to be under predicted. Systemic underprediction of large events by erosion models is also noted by Nearing (1998) who suggested this may be caused by small-scale random variations in soil properties. This is a plausible explanation for the current study, where substantial variability between silt fence observations for this large sediment production period was observed. Both hydrologic unit representation and the difficulty associated incorporating a higher resolution of soil hydraulic or micro-topographic properties into the WEPP framework is a limitation for this and other models which designate relatively large hydrologic response units. Depending on the scale of application, this may be negligible.

At the watershed scale, the model was able to adequately estimate sediment production for both years. Contrary to observations for hillslope sediment loss, the 3 Aug. collection period for catchment sediment yield was lower than the following 10 Aug. collection period. Although the 3 Aug. collection period started after the first documented storm, this event likely still contained a portion of sediment which was made more erodible by the fire. In this case, sediment loss at the hillslope would have a large capture rate by the silt fences, while the channelized suspended fraction of sediment may have been higher than in later events, prompting a lower watershed sediment yield in the settling ponds. The

estimation of the suspended fraction at 50% of total sediment was held constant throughout this study and may contribute to the error in total watershed sediment yield. Furthermore, deposition of sediment below silt fences was observed during this period, which may have been diminished over the 2011 summer period. This may explain the large hillslope sediment loss compared to the catchment sediment yield. Despite discrepancies between individual cleanout periods, the annual observed catchment sediment yield rates of 2.43 Mg ha^{-1} yr^{-1} for 2011 and 0.47 Mg ha^{-1} yr^{-1} for 2012 matched very well with the simulated values of 2.65 Mg ha^{-1} yr^{-1} for 2011 and 0.40 Mg ha^{-1} yr^{-1} for 2012. The calibration of soil properties in hydrologic models is generally susceptible to error (Binley, et al., 1991). During this study, a large effort was placed on representing the distribution of model inputs within the modeling framework to emulate the observed effects of such heterogeneity. Despite this, uncertainty in model parameters remains an issue. Many properties used were estimated or modeled based on current literature and field observations, however due to constraints of past field observations, the true nature of these properties is unknown.

Post-fire hydrology is exceedingly difficult to accurately model due to the evolution of soil hydraulic properties over time, which were initially affected by the fire. During calibration of soil properties for this study, the attempt was made to accurately describe how fire directly affected these properties, however many specific WEPP parameters are affected by multiple physical fire effects. For example, both water repellency and macropore sealing affect the soil hydraulic conductivity, and each evolve differently over time. Whereas water repellency may degrade within a year (Doerr, et al., 2000; Jiménez-Pinilla, et al., 2016), the effects of pore sealing often persist for a much longer duration (Giovannini, et al., 1987). Initial high burn severity saturated hydraulic conductivity of the model presented here is an order of magnitude lower than compared to values reported in the literature. For similar textural classes described here, many authors have reported values ranging from 2 to 20 mm hr^{-1} (Robichaud et al., 2007) or even as high as 100 mm hr^{-1} (Fox & Carrega, 2007). Regarding this, Moody and Ebel (2014) noted a similar trend during model calibration of the HYDRUS-1D model where saturated conductivity was an order of magnitude less than reported values. In this discussion, they suggest that many of these values were produced from artificial rainfall, repacked soil cores, or ponded head instruments which may inaccurately convey the conductivity experienced during natural events. Although an increase

in soil bulk density has been documented post-fire, the high severity bulk density used in the current model is larger than typically found in experimental post-fire data. At 1.9 g cm^{-3}, this represents an increase of 27% from the unburned bulk density reported in the STATSGO database (Table 3.3). While this value is relatively high compared to values reported in the literature for forest environments, Giovannini and Lucchesi (1997) noted increases in bulk density between 8 to 33% with values densities ranging from 1.36 to 1.82 g cm^{-3} for high burn severity clay loams. For the current high gravel content soils, this may be reasonable. Concerning soil water content, many authors have described the apparent changes in field capacity and wilting point of burned soils (Stoof, et al., 2010; Ebel, 2012). These effects are primarily due to changes in organic matter content and particle size, both of which can affect soil water retention.

During hillslope delineation, several concerns arose with the hillslope boundary delineation and slope discretization process performed by the TOPAZ tool. As one of the listed assumptions and possible failures of the model, Garbrecht and Martz (1999) note that calibration of the minimum stream channel length and critical source area parameters to first order streams may produce anomalous artifacts downstream. Conversely, as seen in this study, when attempting to calibrate delineation parameters for these downstream artifacts, the model tended to produce larger hillslopes boundaries than desired. This can be seen in the unburned and low burn severity hillslopes shown in Figure 3.3a, where the stream channel length, and consequently slope width, are larger than 1 km. For this case, these larger hillslopes were located in a relatively unburned portion of the West Willow catchment and likely had a negligible effect in relation to parameter assignment and hydrological processing. Another limitation arose in the slope discretization process. Using both 10 and 30 m DEMs, the GeoWEPP DEM processing with *topwepp* (Flanagan, et al., 2013) program failed to describe the observed concave nature of the toe slopes for Hill 1 and 2. Both these hillslopes displayed a steep ‘s-shape’ slope profile, however the slope definition in the delineation process yielded a convex profile for both. This had implications for the deposition mechanisms within WEPP and prompted the model to over-predict catchment sediment yield.

Uncalibrated validation in the North Thomas catchment shows that the model was able to be transferred to the nearby catchment successfully. The NSE and r^2 values of 0.57 and 0.69 suggest that the model was well able to predict daily average flows, parti qcularly for an

uncalibrated model. The peak flow comparison similarly suggests this with an r^2 value of 0.76. Streamflow data quality for this catchment likely affected the accuracy of the model. These data were collected by an external third-party and were not heavily scrutinized in their raw format. Unknown processing artifacts can be seen in the observed portions of the hydrograph (Figure 3.15), particularly in the baseflow recession in September and October. For the prior months, the baseflow appears appropriate.

Conclusion

Due to the difficulty in collecting post-fire sediment yield and streamflow data there have been few opportunities to assess a process-based hydrologic and soil erosion model at both the hillslope and watershed scales. Understanding the interactions between post-fire soil hydraulic properties, vegetative loss and recovery, precipitation and weather patterns, and downstream hydrologic responses are particularly important for directing effective land management strategies. Furthermore, the spatial scale and spatial patterns in which fire affects landscapes has been shown to dictate many post-fire responses. By applying the WEPP model within a framework that addresses the hillslope-scale variability in burn severity, model simulations may generate more meaningful results. In this application following a stepwise calibration procedure, the WEPP model performed very well at simulating post-fire streamflow, hillslope sediment loss, and watershed sediment yield for the West Willow catchment. The calibration parameters generally agreed with literature values with increases in bulk density and erodibility, decreases in saturated conductivity, field capacity and wilting point moisture content the first year after wildfire. Over the next three years these parameters recovered back to unburned soil conditions as consistent with existing literature. When applied to the nearby North Thomas catchment without further calibration, the model still performed well at capturing peak and daily streamflow. This close agreement indicates that the WEPP model is capable of representing the post-fire hydrologic and erosion response. As it relates to management strategies, this study suggests WEPP can be a powerful tool for assessing post-fire watershed responses, particularly assessment of flooding and erosion risk.

Chapter 4: Data Visualization and Risk Communication Methods

Abstract

Over the past decade, advances in computing and visualization frameworks have facilitated the advancement of many environmental modeling and geographical analysis frameworks. Particularly important for practical applications, numerical environmental models provide a unique and advanced view into our natural systems which can assist land managers by providing accessible, science-based information. Currently, there are many online interfaces for the physically-based hydrologic and sediment transport model, the Water Erosion Prediction Project (WEPP), which facilitate model use for specific scenarios including post-fire treatment, pre-fire fuel management, and nutrient management. While these interfaces are widely used, many lack robust visualization and communication methods. In this chapter, methods are presented to assist in visualization, communication, and processing for various scenarios which are targeted towards geospatial parameterization, topographic representation, and web-mapping frameworks.

Introduction

Online water resource decision support tools can offer managers, policy-makers, and scientists easy access to advanced computing models which may normally have large barriers to adoption (Verma, et al., 2012). By providing server-sided processing power and easy-to-use interfaces, web-based modeling frameworks extend the usability of complex models to a professional audience, giving them the tools to use science-based knowledge to support sensible land management practices (Ferster, 2013). Over the past decade, such online interfaces have grown in popularity through similar ‘Software-as-a-Service’ (SaaS) frameworks which allow users to access a model’s functionality without having to install a program or process files manually (Hossain, et al., 2017).

The WEPP Model Interfaces

The Water Erosion Prediction Project Model (WEPP), a physically-based, hillslope-scale hydrologic and sediment transport model, has been developed and modified to simulate catchment-scale water and sediment yield in undisturbed, disturbed, and burned forest

environments (Robichaud, et al., 2007; Dun, et al., 2009). One of the major benefits to this model is its fully transferable nature, which allows users to call upon a variety of internal and external input databases to run the model in almost any environment across the world. As a traditional executable program, the default version of the WEPP is a Fortran console application that offers customization of hundreds of physically-based parameters. This degree of customization is needed for some advanced users; however, many users may not desire this complexity. To solve this problem many web-based interfaces to the WEPP model following the SaaS framework have been developed for specific use scenarios including post-fire treatment, road sediment delivery, and nutrient loading (Elliot 2004; Brooks, et al., 2016). As a fully transferable, physically-based model, users can call upon a variety of internal and external input databases to run the model in almost any environment across the world. These interfaces allow managers to easily simulate the effects of land use practices or management decisions with minimal effort needed for input creation or understanding of underlying physical mechanisms of the model. Such frameworks avoid the high level of complexity of the full model, yet still provide valuable model output.

The current generation of online spatial WEPP interfaces developed within the past decade allow users to automatically generate inputs and run the WEPP model with the necessary soil, topography, vegetation, and climate files for a given watershed (Frankenberger, et al., 2011; Elliot, et al., 2016). While this automatic process allows the interfaces to be used by a broader audience, and otherwise provides excellent server-sided processing procedures, most lack implementation of robust web-geovisualization and data exploration tools as well as state-of-the-art geovisualization concepts. Although visualization is not specifically necessary in a modeling framework, is considered a key factor in interpreting and understanding model results as well as provide insights that may otherwise be overlooked (Huang & Worboys, 2001). Beyond simple static web-mapping, which allows a user to only view model results, many common web programming libraries and frameworks are available to support the user's experience through an interactive visualization and exploratory data analysis. This includes standard functionality in web-mapping libraries like *OpenLayers* and *Leaflet*, (*openlayers.org*, *leafletjs.com*) or data visualization libraries including *three.js*, *p5.js*, or *d3.js (threejs.org*, *p5js.org*, *d3js.org)*. Functionality provided with these libraries provide a robust toolset to develop any form of visualization desired.

Visualization and Processing Methods

To bridge the apparent gap between web-based WEPP interfaces and state-of-the-art geovisualization techniques, we have developed methods for both data processing and visualization of model components which can been implemented in commonly used *JavaScript* libraries or processed in a *Python* environment (*python.org*). These methods include processing for:

- ❑ Interactive feature selection
- ❑ Linked panes and multiple views
- ❑ Data transferability frameworks
- ❑ 2D and 3D terrain visualizations
- ❑ Topographic abstraction representations

Web Mapping Framework

The basis for an interactive web mapping framework relies on the ability of a user to visualize and interact with geographic data while requiring as few inputs from the user as possible. To this effect, the implementation of these techniques should be tailored to the individual interfaces which they are applied so the developer is able to anticipate what outcomes the user desires. This functionality mimics a traditional GIS environment while providing the flexibility of an online application. Existing online spatial WEPP frameworks offer a static geovisualization method which presents raster and vector map layers using various *JavaScript* libraries with standardized methods (Flanagan, et al., 2013). This technique allows a user to select static maps to visualize, however it offers no interaction of individual features within the map.

Interactive Selections

Both *OpenLayers* and *Leaflet JavaScript* libraries natively allow interactive selection of vector features displayed in a frame. This dynamic interaction follows the general procedure:

1. Select feature in map frame (e.g. basin, hillslope, sub-hillslope selection)
2. Return feature ID from event function
3. Call function with feature ID
4. Update *HTML* to display new information

This general framework can be used to prompt any desired analysis procedure from simple tabular checks on model inputs to hillslope-specific graphical analyses. By allowing a user to select features and instantly re-render features to represent spatial data and display additional desired information relative to the specific feature, we can provide a pathway to explore the model dynamically, similarly to a traditional geographic information system. For example, single hillslope feature is selected and a 'linked pane' within the same view is displayed showing relevant information at this stage in processing. Information will be updated to include other attributes as the user continues the model workflow (Figure 4.1 and 4.2). A *JavaScript* framework which accomplishes this can be found in Appendix C. In this example, a static image is displayed which corresponds to the selected hillslope.

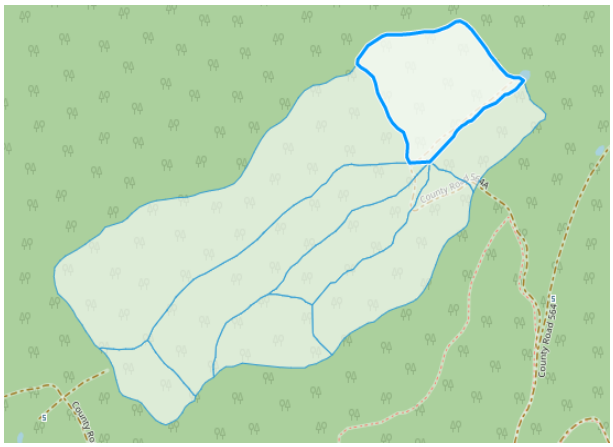

Figure 4.1 Watershed vector layer with 8 hillslopes shown in a default OpenLayers window.

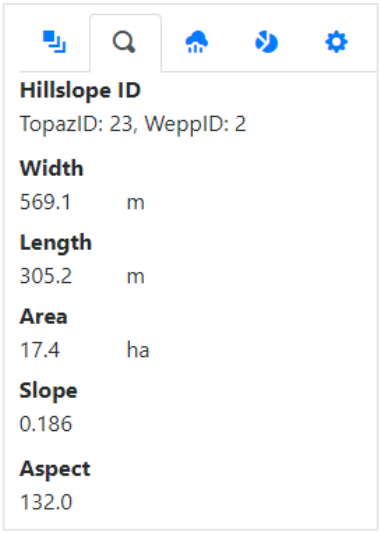

Figure 4.2 Information pane displaying hillslope information (WEPP Cloud, 2018)

Linked Views

This process of feature selection and immediate feedback relies on an interrupted workflow. Immediate feedback processes have been a staple of traditional data analysis and GIS software. In these applications, dynamic 'linking' and 'brushing' of a view is used as a powerful organizational technique for both processing of inputs and visualization of outputs (Anselin, et al., 2005). In this process, when one feature is selected by a user, an immediate connection is made with another component in the same view on the screen. Brushing is a similar concept where multiple features may be selected or 'brushed' over. Further application of this selection-display process in an online WEPP framework can be used to prompt processing of inputs at the hillslope-scale, which may be necessary if automatically generated inputs are found to be objectionable.

Topographic Abstraction

All numerical models are simplifications of a system. As such, we rely on varying scales of conceptual abstractions to represent the physical mechanisms at play in a simplified system. With hillslope-scale hydrological models like WEPP, topographic abstraction is a key driver of many physical processes including runoff generation, sediment transport, and deposition (Grayson, et al., 1992). The standard abstraction process for creating topographic inputs commonly entails elevation mapping, channel and catchment delineation, hydrologic response unit discretization, and finally, slope profile description. In the WEPP model, the hydrologic units take the form of a rectangular representative hillslope which allows the model to describe the slope profile (top to bottom), but not curvature (left to right) (Flanagan & Nearing, 1995). After we define these rectangular hillslopes, we must ensure the underlying key topographic features that drive hydrological responses were not over-generalized or lost during the abstraction process. Many WEPP web interface variants lack this type of intermediate check which opens the possibility for unnecessary errors. The pre-processing visualization methods described here focus on topographic representations at multiple scales, which allow a user to view key topographic abstractions in two and three dimensions.

2D Hillslope Visualization

The WEPP model's most basic topographic feature is represented as a rectangular hillslope with a fixed length and width. The slope profile which this rectangular hillslope represents drives many of the mechanistic processes affecting runoff and sediment transport estimations. Because of this, it is important to ensure the algorithms which abstract a representative hillslope from the digital elevation model are as accurate as possible. Within a defined hillslope, overland flow elements (OFEs) can also be defined which represent sub-units of a hillslope with homogenous management and soil inputs. The default executable version of WEPP provides this feature when running single hillslopes, however this feature has not yet been implemented into many of the web interfaces of WEPP. To generate these

visualizations, a Python-based script was developed which reads a standard WEPP slope file and other input properties including OFE burn severity and returns lists of coordinates to plot each feature in a web-framework as well as a standalone graphics file. Images are generated with this process including defined WEPP OFEs with associated burn severity (Figure). With this visualization of the basic topographic modeling unit, it is possible to visualize the representation and check against *a posteriori* observation.

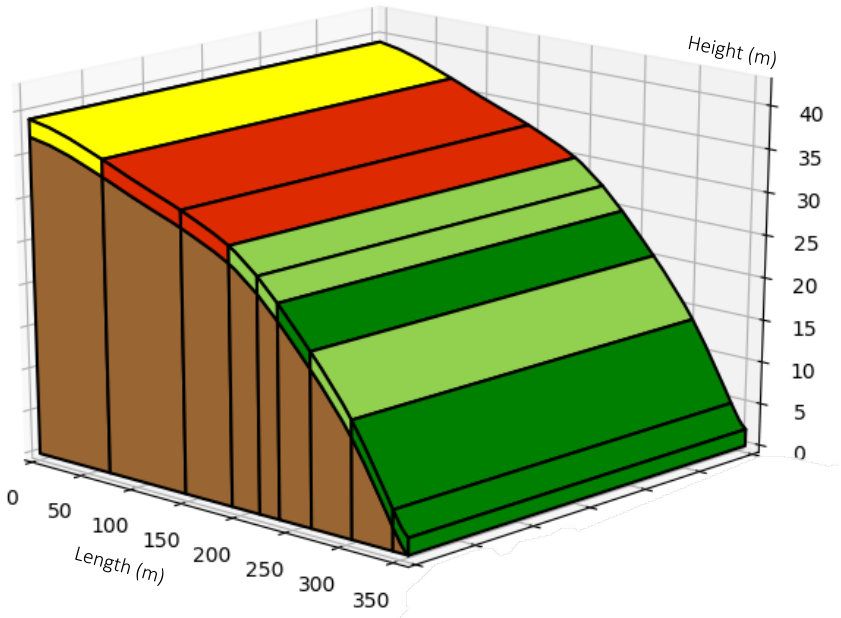

Figure 4.3 Example of a representative hillslope visualization

Case Study Application – This hillslope visualization framework was applied to hillslopes within the West Willow catchment (see Chapter 3) to examine the TOPAZ delineation for errors or artifacts. The original profile delineation process yielded a convex slope profile (Figure 4.4a) which was inaccurate when compared to field observations and the elevation model. In reality, this hillslope was characterized by an 's-shaped' profile (Figure 4.4b). For this case, the original hillslope profile had severe implications for the erosion and deposition mechanisms within the model, which caused a large overestimation of sediment.

a) Original profile b) Modified profile

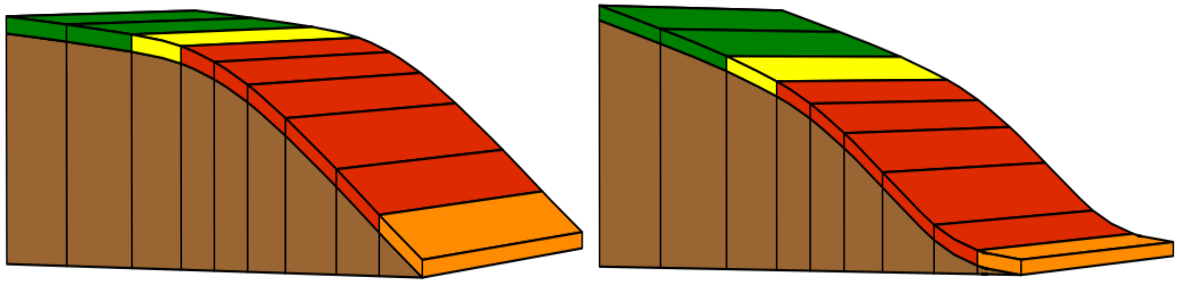

Figure 4.4 a) Original and b) modified slopes for a hillslope in the West Willow catchment

3D Terrain Visualization

Contrary to viewing terrain abstraction in a 2D profile configuration, it may often be helpful to visualize hillslopes in their 3D state. This method extends beyond the topographic characterization offered by WEPP as a 2D model, while allowing a user to recognize possible limitations in their hillslope delineation configuration. By comparing WEPP representative hillslopes to a 3D digital elevation model (DEM) which each hillslope was defined from, we can ensure such limitations are not being unreasonably surpassed. For example, parameters which direct channel delineation often need to be calibrated for a specific landscape. If inappropriate parameters are chosen, the hillslope delineation routines may be unable to adequately represent the defined topography through a rectangular representative hillslope, which will impact modeling results. This effect may be difficult notice using the existing interface maps yet can be easily recognized when compared in three dimensions.

The module developed here enables a user to generate and visualize subset watershed and hillslope DEM subsections. When a visualization is called through the hillslope selection process, the corresponding DEM which has been clipped to hillslope boundaries will be shown using *JavaScript* with the *three.js* library. Preprocessing of raster DEM files is completed in *Python* using the *GDAL* library.

Interface Integration

Existing online spatial WEPP interfaces have been published previously and seen modest use by land managers. This includes generalized online versions of the GeoWEPP interface processing scheme described by Renschler (2003) which incorporate server-based backend processing flow with web client-based interfaces (Frankenberger, et al., 2011). Other geographically specialized and specific scenario interfaces have since been developed including The Great Lakes Basin, the Lake Tahoe Basin, and post-fire scenarios (Elliot, et al., 2016). Many of these existing interfaces were developed with a *PHP* processing scheme (*php.net*) using the open-source packages of *OpenLayers* for geovisualization and *GDAL (*Geospatial Data Abstraction Library; *gdal.org*) for geoprocessing. Using a similar scheme, Lew and Dobre (*in preparation*) have developed an online spatial WEPP interface which includes a *Python* and *GDAL* backend and *Python* generated *HTML* frontend with *Leaflet*

geovisualization. The methods described were designed to be adapted into either current or future frameworks.

Conclusion

The methods outlined in this chapter seek to facilitate communication of the WEPP model's inputs and processing framework. Current online mapping frameworks allow model interfaces to provide a more rich and robust interaction between the user and the model's front end and should be implemented into all current or future interfaces. Furthermore, visual representations of many model properties including the topographic representations allow a user to ensure correct model processing. This framework can be extended to other model inputs which can allow for a greater user experience.

Chapter 5: Synthesis

Wildfire is poised to become an increasingly influential component of our daily lives over the next century in the Western United States and other fire-prone areas. Shifting climate patterns are likely to drive changes in the historical fire regimes at the global scale, and we need to be able to adapt to these changes. Beyond the direct effects of fire, the downstream cascading consequences of post-fire flooding, erosion, and debris flow will have lasting effects on our environment and our communities. Many of the processes which control post-fire hydrology are well understood, and the development of predictive modeling tools has seen many successes for guiding post-fire hydrological recovery. With the increasing use of this predictive power, more robust tools are needed to efficiently guide cost-effective management and mitigation strategies to reduce future catastrophic hydrologic scenarios.

In the preceding chapters, the WEPP model was shown to be capable of simulating post-fire hydrology and erosion patterns at the watershed scale. A large focus of this thesis was to incorporate the hydraulic connectivity of soil burn severity into the model framework. The results shown in Chapter 2 suggest including representation of these spatial burn severity patterns into the model has great implications for the site-specific simulations. This provides a unique opportunity for the further development and use of the WEPP model for post-fire simulations, specifically for management scenarios. With the framework described here, it is possible to simulate targeted erosion mitigation practices within the WEPP model with a higher degree of spatial and predictive accuracy for large catchments with relatively quick model simulations. This can be applied for both post-fire mitigation strategies as well as pre-fire fuel treatment planning to protect sensitive areas from a future fire threat.

One of the unique benefits of the WEPP model is its ability to easily transfer between different climatic zones and ecoregions. Chapter 3 demonstrated an application of this model to capture post-fire hydrology and erosion responses in the semi-arid Southwest which was characterized by a high intensity precipitation summer monsoon season. The performance of the model in both calibrated and uncalibrated simulations shows that WEPP can be a powerful tool for answering post-fire land management questions. While this model assessment here was targeted at application of a continuous daily simulation with real-world data, these results may be even more important for simulations in a probabilistic model framework, similar to

the ERMiT interface. In scenarios which managers need to know the most cost-effective treatment to prevent hillslope erosion from a future storm or decide which catchments and drainage networks will be likely to see massive flooding, the accuracy and validity of the model is a chief concern. For large-scale watershed simulations, the methods and results in Chapter 2 and 3 present a framework which can benefit both the spatial accuracy as well as simulation validity. Many of the visualization and processing techniques discussed in Chapter 4 can be incorporated into existing model interfaces to provide a more robust user experience while also enhancing model accuracy through immediate user feedback and visualization strategies.

Moving forward, further development and experimentation with watershed-scale post-fire WEPP simulations strategies is needed to expand the validity, transferability, and accuracy of the model. Over the past many decades, researchers have experimented and collected a bounty of knowledge on how fire affects soil. Hydrological applications including WEPP must be able to synthesize this body of work to guide internal parameterization schemes without over-generalizing. While this is a difficult task, continued research which describes the observed relationships between pre-fire conditions, soil burn severity, and soil hydraulic properties would undoubtedly benefit modeling efforts. Using the framework described herein, hillslope-scale patterns and topographically-driven fire effects should also be considered when parameterizing these models.

References

Abatzoglou, J. T., & Kolden, C. A. (2013). Relationships between climate and macroscale area burned in the western United States burned in the western United States. *International Journal of Wildland Fire, 22*(7), 1003-1020.

Agee, J. K. (1996). *Fire ecology of Pacific Northwest forests.* Island Press.

Anselin, L., Syabri, I., & Youngihn, K. (2005). GeoDa: an introduction to spatial data analysis. *Geographical Analysis, 38*(1), 5-22.

Beck, H. E., vanDijk, A. I., Miralles, D. G., de Jeu, R. A., Bruijnzeel, L. A., Mcvicar, T. R., & Schellekens, J. (2013). Global patterns in base flow index and recession based on streamflow observations from 3394 catchments. *Water Resources Research, 49*, 7843-7863.

Beck, M. B., Kleissen, M. F., & Wheatler, H. S. (1990). Identifying flow paths in models of surface water acidification. *Reviews of Geophysics, 28*(2), 207-230.

Beven, K. J., & Kirkby, M. J. (1979). A physically based, variable contributing area model of basin hydrology. *Hydrological Sciences Bulletin, 24*(1), 43-69.

Bigler, C., Kulakowski, D., & Veblen, T. T. (2005). Multiple disturbance interactions and drought influence fire severity in Rocky Mountain subalpine forests. *Ecology, 86*(11), 3018-3029.

Binley, A. M., Beven, K. J., Calver, A., & Watts, L. G. (1991). Changing responses in hydrology: assessing the uncertainty in physically based model predictions. *Water Resources Research, 27*(6), 1253-1261.

Birch, D. S., Morgan, P., Kolden, C. A., Abatzoglou, J. T., Dillon, G. K., Hudak, A. T., & Smith, A. M. (2015). Vegetation, topography and daily weather influenced burn severity in central Idaho and western Montana. *Ecosphere, 6*(1), 17.

Boll, J., Brooks, E. S., Crabtree, B., Dun, S., & Steenhuis, T. S. (2015). Variable source area hydrology modeling with the Water Erosion Prediction Project model. *Journal of the American Water Resources Association, 51*(2), 330-342.

Bone, E. D. (2017). *Effects of burn severity on stream buffer management for post-fire hillslope erosion in the inland Northwest mountain ranges, USA (M.S. Thesis).* Moscow, ID: University of Idaho.

Bracken, L. J., & Croke, J. (2007). The concept of hydrological connectivity and its contributions to understanding runoff-dominated geomorphic systems. *Hydrological Processes, 21*, 1749-1763.

Bristow, K. L., & Campbell, G. S. (1984). On the relationship between incoming solar radiation and daily maximum and minimum temperature. *Agricultural and Forest Meteorology, 31*, 159-166.

Brooks, E. S., Dobre, M., Elliot, W. J., Wu, J. Q., & Boll, J. (2016). Watershed-scale evaluation of the Water Erosion Prediction Project (WEPP) model in the Lake Tahoe basin. *Journal of Hydrology, 533*, 389-402. doi:10.1016/j.jhydrol.2015.12.004

Cawson, J. G., Sheridan, G. J., Smith, H. G., & Land, P. N. (2013). Effects of fire severity and burn patchiness on hillslope-scale surface runoff, erosion and hydrologic connectivity in a prescribed burn. *Forest Ecology and Management, 310*, 219-233.

Cerdà, A., & Robichaud, P. R. (2009). Fire effects on soil infiltration. In *Fire effects on soil and restoration strategies* (pp. 81-103). Enfeld, NH: Science Publishers.

Certini, G. (2005). Effects of fire on properties of forest soils: a review. *Oecologia, 143*(1), 1-10.

Cocke, A. E., Fulé, P. Z., & Crouse, J. E. (2005). Comparison of burn severity assessments using Differenced Normalized Burn Ratio and ground data. *International Journal of Wildland Fire, 14*, 189-198.

Covert, A. S. (2003). *Accuracy assessment of WEPP-based erosion models on three small, harvested and burned forest watersheds (M.S. Thesis).* Moscow, ID: University of Idaho.

De Santis, A., & Chuvieco, E. (2007). Burn severity estimation from remotely sensed data: Performance of simulation versus empirical models. *Remote Sensing of Environment, 108*, 422-435.

DeBano, L. F. (1981). *Water repellent soils: a state-of-the-art. Gen. Tech. Rep. PSW-46.* Berkeley, CA: US Department of Agriculture, Forest Service, Pacific Southwest Forest and Range Exp. Stn. 21.

DeBano, L. F. (1996). *Formation of non-wettable soils: Involves heat transfer mechanisms* (Vol. 132). Pacific Southwest Forest & Range Experiment Station.

DeBano, L. F. (2000). The role of fire and soil heating on water repellency in wildland environments: a review. *Journal of Hydrology, 231-232*, 195-206.

Dillon, G. K., Holden, Z., Morgan, P., Crimmins, M., Heyerdahl, E., & Luce, C. (2011). Both topography and climate affected forest and woodland burn severity in two regions of the western US, 1984 to 2006. *Ecosphere, 2*(12), 130.

Doerr, S. H., Shakesby, R. A., & MacDonald, L. H. (2009). Soil water repellency: a key factor in post-fire erosion. In *Fire Effects on Soil and Restoration Strategies* (pp. 197-223). Enfield, NH: Science Publishers.

Doerr, S. H., Shakesby, R. A., & Walsh, R. P. (2000). Soil water repellency: its causes, characteristics and hydro-geomorphological significance. *Earth-Science Reviews, 51*, 33-65.

Dun, S., Wu, J. Q., Elliot, W. J., Robichaud, P. R., Flanagan, D. C., Frankenberger, J. R., . . . Xu, A. C. (2009). Adapting the Water Erosion Prediction Project (WEPP) model for forest applications. *Journal of Hydrology, 366*, 46-54.

Ebel, B. A. (2012). Wildfire impacts on soil-water retension in the Colorado Front Range, United States. *Water Resoureces Research, 48*. doi:10.1029/2012WR012362

Elliot, W. J. (2004). WEPP Internet interfaces for forest erosion prediction. *Journal of the American Water Resources Association, 40*(2), 299-309.

Elliot, W. J., & Foltz, M. (2001). Validation of the FS WEPP interfaces for forest roads and disturbance. #01-8009. *ASAE Annual Meeting.* Sacramento: American Society of Agricultural and Biological Engineers.

Elliot, W. J., & Robichaud, P. R. (2011). Risk-based erosion assessment: application to forest watershed management and planning. In R. P. Morgan, *Handbook of Erosion Modelling* (pp. 313-323). West Sussex, UK: Wiley-Blackwell.

Elliot, W. J., Miller, M. E., & Enstice, N. (2016). Targeting forest management through fire and erosion modelling. *International Journal of Wildland Fire, 25*, 876-887.

Eppler, M. J., & Burkhard, R. A. (2007). Visual representations in knowledge management: framework and cases. *Journal of Knowledge Management, 11*(4), 112-122.

Escuin, S., Navarro, R., & Fernandez, P. (2008). Fire severity assessment by using NBR (Normalized Burn Ratio) and NDVI (Normalized Difference Vegetation Index)

derived from LANDSAT TM/ETM images. *International Journal of Remote Sensing* (29), 1053-1073.

Fauria, M. M., Michaletz, S. T., & Johnson, E. A. (2011). Predicting climate change effects on wildfires requires linking processes across scales. *Wiley Interdisciplinary Reviews: Climate Change, 2*(1), 99-112.

Fernández, C., & Vega, J. A. (2016). Modelling the effect of soil burn severity on soil erosion at hillslope scale in the first year following wildfire in NW Spain. *Earth Surface Processes and Landforms, 41*, 928-935.

Ferster, B. (2013). *Interactive visualization: Insight through inquiry.* Cambridge, MA: MIT Press.

Flanagan, D. C., & Nearing, M. A. (1995). *USDA-Water Erosion Prediction Project hillslope profile and watershed model documentation.* West Lafayette, Indiana.: USDA-Agricultural Research Service, National Soil Erosion Research Laboratory (NSERL).

Flanagan, D. C., Frankenberger, J., Cochrane, T., & Renschler, C. S. (2013). Geospatial application of the Water Erosion Prediction Project (WEPP) model. *Transactions of the ASABE, 52*(2), 591-601.

Foglia, L., Hill, M. C., Mehl, S. W., & Burlando, P. (2009). Sensitivity analysis, calibration, and testing of a distributed hydrological model using error-based weighting and one objective function. *Water Resources Research, 45*.

Fox, D. M., Darboux, F., & Carrega, P. (2007). Effects of fire-induced water repelleny on soil aggregate stability, splash erosion, and saturated hydraulic conductivity for different size fractions. *Hydrological Processes, 21*, 2377-2384.

Fox, D., & Carrega, P. (2007). Effects of fire-induced water repellency on soil aggregate stability, splash erosion, and saturated hydraulic conductivity for different size fractions. *Hydrological Processes, 21*, 2377-2384.

Frankenberger, J. R., Dun, S., Flanagan, D. C., Wu, J. Q., & Elliot, W. J. (2011). Development of a GIS interface for WEPP model applications to Great Lakes forested watersheds. *International Symposium on Erosion and Landscape Evolution.* Anchorage: American Society of Agricultural and Biological Engineers.

Garbrecht, J., & Martz, L. W. (1999). *An automated digital landscape analysis tool for topographic evaluation, drainage identification, watershed segmentation, and subcatchment parameterization.* El Reno, OK: USDA, Agricultural Research Service.

Giovannini, G., & Lucchesi, S. (1997). Modifications introduced in soil physico-chemical parameters by experimental fires at different intensities. *Soil Science, 162*(7), 479-486.

Giovannini, G., Lucchesi, S., & Giachetti, M. (1987). The natural evolution of a burned soil: A three-year investigation. *Soil Science, 143*, 202-226.

Gonçalves, A. B., Vieira, A., Leite, F. F., Lourenço, L., Botelho, H., Fernandes, P., . . . Cerdà, A. (2011). *Field trip guidebook : 3rd international meeting of fire effects on soil properties.* (A. B. Gonçalves, & A. Vieira, Eds.) Núcleo de Investigação em Geografia e Planeamento (NIGP).

Gottfried, G. J. (1983). Stand changes on a southwestern mixed conifer watershed after timber harvesting. *Journal of Forestry, 83*(5), 311-316.

Gottfried, G. J. (1991). Moderate timber harvesting increases water yields from an Arizona mixed confier watershed. *Water Resoureces Bullitin, 27*(3), 537-547.

Grayson, R. B., Moore, I. D., & McMahon, T. A. (1992). Physically based hydrologic modelling: is the concept realistic? *Water Resources Research, 26*(10), 2659-2666.

Hallema, D. W., Sun, G., Bladon, K. D., Norman, S. P., Caldwell, P. V., Liu, Y., & McNulty, S. G. (2017). Regional patterns of postwildfire streamflow response in the Western United States: The importance of scale-specific connectivity. *Hydrological Processes, 31*, 2582-2598.

Hargreaves, G. H., & Samani, Z. A. (1985). Reference crop evapotranspiration from temperature. *Applied Engineering in Agriculture*, 96-99.

Heede, B. H. (1985). Channel adjustments to the removal of log steps: an experiment in a mountain stream. *Environmental Management, 9*(5), 427-432.

Heede, B. H. (1987). Overland flow and sediment delivery five years after timber harvest in a mixed conifer forest, Arizona, USA. *Journal of Hydrology, 91*, 205-216.

Heede, B. H. (1991). Response of a stream in disequilibrium to timber harvest. *Environmental Management, 15*(2), 251-255.

Holden, Z. A., & Jolly, W. M. (2011). Modeling topographic influences on fuel moisture and fire danger in complex terrain to improve wildland fire management decision support. *Forest Ecology, 262*(12), 2133-2141.

Holden, Z. A., Morgan, P., & Evans, J. S. (2009). A predictive model of burn severity based on 20-year satellite-inferred burn severity data in a large southwestern US wilderness area. *Forest Ecology and Management, 258*, 2399-2406.

Hossain, M. M., Wu, R., Painumkal, J. T., Kettouch, M., Luca, C., Dascalu, S. M., & Harris, F. C. (2017). Web-service framework for environmental models. *Institute of Electrical and Electronics Engineers*, 104-109.

Huang, B., & Worboys, M. F. (2001). Dynamic modelling and visualization on the internet. *Transactions in GIS, 5*(2), 131-139.

Hubbard, K. G., Mahmood, R., & Carlson, C. (2003). Estimating daily dew point temperature for the northern great plains using maximum and minimum temperature. *Agronomy Journal, 95*, 323-328.

Hudak, A. T., Morgan, P., Bobbitt, M. J., SMith, A. M., Lewis, S. A., Lentile, L. B., . . . McKinley, R. A. (2007). The relationship of multispectral satellite imagery to immediate fire effects. *Fire Ecology, 3*(1), 64-90.

Jenks, G. F. (1967). The data model concept in statistical mapping. *International Yearbook of Cartography, 7*, 186-190.

Jiménez-Pinilla, P., Lozano, E., Mataix-Solera, J., Arcenegui, V., Jordán, A., & Zavala, L. M. (2016). Temporal changes in soil water repellency after a forest fire in a Medeterranean calcareous soil: Influence of ash and different vegetation type. *Science of the Total Environment, 572*, 1252-1260.

Jonasson, S. (1988). Evaluation of the point intercept method for the estimation of plant biomass. *Oikos, 52*(1), 101-106.

Keeley, J. E. (2009). Fire intensity, fire severity and burn severity: a brief review and suggested usage. *International Journal of Wildland Fire, 18*, 116-126.

Key, C. H., & Benson, N. C. (2006). *Landscape Assessment (LA) Sampling and Analysis Methods.* Gen. Tech. Rep. RMRS-GTR-164-CD: USDA Forest Service, Rocky Mountain Research Station, Fort Collins, CO.

Kimball, J. S., Running, S. W., & Nemani, R. (1997). An imporved method for estimating surface humidity from daily mimimum temperature. *Agricultural and Forest Meterology, 85*, 87-98.

Krause, P., Boyle, D. P., & Bäse, F. (2005). Comparison of different efficiency criteria for hydrological model assessment. *Advances in Geosciences, 5*, 89-97.

Larsen, I. J., & MacDonald, L. H. (2007). Predicting postfire sediment yields at the hillslope scale: Testing RUSLE and Disturbed WEPP. *Water Resources Research, 43*(11).

Larsen, I., MacDonald, L., Brown, E., Rough, D., Welsh, M., Pietraszek, J., . . . Schaffrath, K. (2009). Causes of post-fire runoff and erosion: water repellency, cover, or soil sealing? *Soil Science Society of America Journal, 73*(4), 1393-1407.

Lentile, L. B., Holden, Z. A., Smith, A. M., Falkowski, M. J., Hudak, A. T., Morgan, P., . . . Benson, N. C. (2006). Remote sensing techniques to assess active fire characteristic and post-fire effects. *International Journal of Wildland FIre, 15*, 319-345.

Letey, J. (2001). Causes and consequences of fire-induced soil water repellency. *Hydrological Processes, 15*, 2867-2875.

Letty, J. (2005). Water-repellent soils. In *Encyclopedia of Soils in the Environment* (pp. 301-306). Oxford, UK: Elsevier.

Lewis, S. A., Wu, J. Q., & Robichaud, P. R. (2006). Assessing burn severity and comparing soil water repellency, Hayman Fire, Colorado. *Hydrological Processes, 20*, 1-16.

Miller, J. D., & Thode, A. E. (2007). Quantifying burn severity in a heterogenous landscape with a relative version of the delta Normalized Burn Ratio (dNBR). *Remote Sensing of Environment, 12*(1), 66-80.

Miller, M. E., Elliot, W. J., Billmire, M., Robichaud, P. R., & Endsley, K. A. (2016). Rapid-response tool and datasets for post-fire remediation: linking remote sensing and process-based hydrological models. *International Journal of Wildland Fire, 25*, 1061-1073.

Miller, M. E., MacDonald, L. H., Robichaud, P. R., & Elliot, W. J. (2011). Predicting post-fire hillslope erosion in forested lands of the western United States. *International Journal of Wildland Fire, 20*, 982-999.

Moody, J. A., & Ebel, B. (2014). Infiltration and runoff generation processes in fire-affected soils. *Hydrological Processes, 28*, 3432-3453.

Moody, J. A., Ebel, B. A., Nyman, P., Martin, D. A., Stoof, C. R., & McKinley, R. (2016). Relations between soil hydraulic properties and burn severity. *International Journal of Wildland Fire, 25*, 279-293.

Moody, J. A., Martin, D. A., Haire, S. L., & Kinner, D. A. (2008). Linking runoff response to burn severity after a wildfire. *Hydrological Processes, 22*, 2063-2074.

Moody, J. A., Shakesby, R. A., Robichaud, P. R., Cannon, S. H., & Martin, D. A. (2013). Current research issues related to post-wildfire runoff and erosion processes. *Earth-Science Reviews, 122*, 10-37.

Morgan, P., Keane, R. E., Dillon, G. K., Jain, T. B., Hudak, A. T., Karau, E. C., . . . Strand, E. K. (2014). Challenges of assessing fire and burn severity using field measures, remote sensing and modelling. *International Journal of Wildland FIre, 23*, 1045-1060.

Nagy, R., Fusco, E., Bradley, B., Abatzoglou, J. T., & Balch, J. (2018). Human-related ignitions increase the number of large wildfires across US ecoregions. *Fire, 1*(1).

Nash, J. E., & Sutcliffe, J. V. (1970). River flow forecasting through conceptual models. *Journal of Hydrology, 10*, 282-290.

Ndlovu, L. S. (1994). *Weather data generation and its use in estimating evapotranspiration (Ph.D. Dissertation).* Pullman, WA: Washington State University.

Nearing, M. A. (1998). Why soil erosion models over-predict small soil losses and under-predict large soil losses. *Caten, 32*(1), 15-22.

NOAA. (2017). Precipitation Frequency Data Server (PFDS). Silver Spring, MD: National Oceanic and Atmospheric Administration National Wearther Service. Retrieved May 20, 2018, from https://hdsc.nws.noaa.gov/hdsc/pfds/

NRCS. (2017). *Web Soil Survey.* USDA Natural Resources Conservation Service. Retrieved February 5, 2017, from https://websoilsurvey.sc.egov.usda.gov

Parks, S. A., Miller, C., Abatzoglou, J. T., Holsinger, L. M., Parisien, M.-A., & Doborwski, S. Z. (2016). How will climate change affect wildland fire severity in the western US. *Environmental Research Letters, 11*.

Parsons, A., Robichaud, P. R., Lewis, S. A., Napper, C., & Clark, J. T. (2010). *Field guide for mapping post-fire soil burn severity.* Gen. Tech. Rep. RMRS-GTR-243.: USDA, Forest Service, Rocky Mountain Research Station. Fort Collins, CO.

Pierson, F. B., Robichaud, P. R., Moffet, C. A., Spaeth, K. E., Hardegree, S. P., Clark, P. E., & Williams, C. J. (2008). Fire effects on rangeland hydrology and erosion in a steep sagebrush-dominated landscape. *Hydrological Processes, 22*, 2916-2929. doi:10.1002/hyp.6904

Pringle, C. (2003). What is hydrologic connectivity and why is it ecologically important? *Hydrological Processes, 17*, 2685-2689.

Renschler, C. S. (2003). Designing geo-spatial interfaces to scale process models: the GeoWEPP approach. *Hydrological Processes, 17*, 1005-1017.

Robichaud, P. R. (2000). Fire effects on infiltration rates after prescribed fire in Northern Rocky Mountain forests, USA. *Journal of Hydrology, 231-232*(2000), 220-229.

Robichaud, P. R., & Brown, R. E. (2002). *Silt fences: an economical technique for measuring hillslope soil erosion.* Gen. Tech. Rep. RMRS-GTR-94. : USDA, Forest Service, Rocky Mountain Research Station. Fort Collins, CO.

Robichaud, P. R., & Miller, S. M. (2000). Spatial interpolation and simulation of post-burn duff thickness after prescribed fire. *International Journal of Wildland Fire, 9*(2), 137-143.

Robichaud, P. R., & Monroe, T. M. (1997). *Spatially-varied erosion modeling using WEPP for timber harvested and burned hillslopes.* Paper No. 97-5015. ASAE Annual International Meeting. American Society of Agricultural. St. Joseph, MI.

Robichaud, P. R., Elliot, W. J., Frederick, P. B., David, H., & Moffet, C. A. (2014). Erosion Risk Management Tool (ERMiT). Moscow, ID. Retrieved February 30, 2017, from https://forest.moscowfsl.wsu.edu/fswepp

Robichaud, P. R., Elliot, W. J., Lewis, S. A., & Miller, M. E. (2016). Validation of a probabilistic post-fire erosion model. *International Journal of Wildland Fire, 25*, 337-350.

Robichaud, P. R., Pierson, F. B., & Brown, R. E. (2007). *Runoff and erosion effects after prescribed fire and wildfire on volcanic ash-cap soils.* Proceedings RMRS-P-44: USDA Forest Service.

Shakesby, R. A., & Doerr, S. H. (2006). Wildfire as a hydrological and geomorphological agent. *Earth Science Reviews, 74*, 269-307.

Shakesby, R. A., Moody, J. A., Martin, D. A., & Robichaud, P. R. (2016). Synthesising empirical results to improve predictions of post-wildfire runoff and erosion response. *International Journal of Wildland Fire, 25*, 257-261.

Soudani, K., Hmimina, G., Delpierre, N., Pontailler, J. Y., Aubinet, M., Bonal, D., . . . Grandcourt, A. (2012). Ground-based network of NDVI measurements for tracking temportal dynamics of canopy structure and vegetation phenology in different biomes. *Remote Sensing of Environment, 123*, 234-245.

Srivastava, A., Wu, J. Q., Elliot, W. J., Brooks, E. S., & Flanagan, D. C. (2017). Modeling streamflow in a snow-dominated forest watershed using the Water Erosion Prediction Project (WEPP) model. *Transactions of the ASABE, 60*(4), 1171-1187.

Srivastava, A., Wu, J., Elliot, W. J., Brooks, E. S., & Flanagan, D. C. (2018, in press). A simulation study to estimate effects of wildfire and forest management on hydrology and sediment in a forested watershed, Northwestern USA. *ASABE*.

Stoof, C. R., Gevaert, A. I., Baver, C., Hassanpour, B., Morales, V., Zhang, W., . . . Steenhuis, T. S. (2016). Can pore-clogging by ash explain post-fire runoff? *International Journal of Wildland Fire, 25*(3), 294-305.

Stoof, C. R., Wesseling, J. G., & Ritsema, C. J. (2010). Effects of fire and ash on soil water retention. *Geoderma, 159*(3-4), 276-285.

Sun, A. (2013). Enabling collaborative decision-making in watershed management using cloud-computing services. *Environmental Modelling & Software*, 93-97.

Turowski, J. M., Rickenmann, D., & Dadson, S. J. (2010). The partitioning of the total sediment load of a river into suspended load and bedload: a review of empirical data. *Sedimentology, 57*, 1126-1146.

Úbeda, X., & Cerdá, A. (2011). The effects of fire on soil properties. In A. B. Gonçalves, *Field trip guidebook : 3rd International Meeting of Fire Effects on Soil Properties* (pp. 45-68). Núcleo de Investigação em Geografia e Planeamento (NIGP).

USDA Forest Service. (2017). *Burned Area Emergency Response*. Retrieved Janurary 1, 2017, from Remote Sensing Applications Center: https://www.fs.fed.us/eng/rsac/baer

USGS. (2015). National Elevation Dataset. Retrieved July 1, 2017, from https://lta.cr.usgs.gov/NED

USGS. (2017). *Landsat-7*. Retrieved Janurary 1, 2017, from https://landsat.usgs.gov/

Verma, S., Verma, R. K., Singh, A., & Naik, N. S. (2012). Web-based GIS and desktop open source GIS software: an emerging innovative approach for water resources management. *Advances in Computer Science, Eng. & Appl.*, 1061-1074.

Wagenbrenner, J. W. (2013). *Post-fire stream channel processes: Changes in runoff rates, sediment delivery across spatial scales, and mitigation effectiveness (Ph.D. Dissertation).* Retrieved from Washington State University.

Wagenbrenner, J. W., & Robichaud, P. R. (2014). Post-fire bedload sediment delivery across spatial scales in the interior western United States. *Earth Surface Processes and Landforms, 39*, 865-876. doi:10.1002/esp.3488

Wang, L., Wu, J. Q., Elliot, W. J., Dun, S., & Fiedler, F. R. (2010). *Implementation of channel-routing routines in the Water Erosion Prediction Project (WEPP) model.* San Francisco, CA: Society for Industrial and Applied Mathematics Conference on Mathematics for Industry.

Weiss, A. D. (2001). *Topographic position and landforms analysis.* San Diego, CA: Poster presentation, ESRI user conference.

WEPP Cloud. (2018). *WEPP Cloud*. Retrieved July 15, 2018, from https://wepp1.nkn.uidaho.edu/weppcloud/

Westerling, A. L., Hidalgo, H. G., Cayan, D. R., & Swetnam, T. W. (2006). Warming and earlier spring increase western US forest wildfire activity. *Science, 313*, 940-943.

Appendix A

The following methods were used to estimate daily solar radiation ($S_t; MJ\ m^{-2}\ d^{-1}$) and dew point ($T_{dew}; C$). Solar radiation was calculated using the difference between minimum and maximum daily air temperature described by Bristow and Campbell (1984) with modifications to allow for seasonal variation as noted by Ndlovu (1994)

$$S_t = 277.7(T_t * S_0) \tag{A.1}$$

for the atmospheric transmission rate, T_t as

$$T_t = A\left(1 - e^{-B\Delta T^C}\right) \tag{A.2}$$

where ΔT is the difference of daily maximum and minimum temperatures, A, B, and C are empirical parameters which are calibrated using observed data at the study location. These parameters were fitted to nearby weather stations in Alpine, AZ.

The extraterrestrial solar radiation, $S_0;\ MJ\ m^{-2}\ d^{-1}$ was calculated as a function of the solar declination angle, $\delta\ (rad)$, the latitude, $\lambda\ (rad)$, the half-day length $h\ (rad)$, and the day of year, DOY as:

$$S_0 = \frac{117.5(h \sin\lambda \sin\delta + \cos\lambda \cos\delta \sin h)}{\pi} \tag{A.3}$$

$$\delta = \sin^{-1}(0.39785 \sin(4.869 + 0.0172 * DOY + 0.03345 \sin(6.224 + 0.0172 * DOY)))$$

$$h = \cos^{-1}(-\tan\lambda \tan\delta)$$

Daily dew point was similarly modeled using an empirical regression described by Kimball, et al. (1997), which is based on the daily minimum temperature as follows:

$$T_{dew} = \left(T_{min,K}\right)(-0.127 + 1.121(1.003 - 1.444EF + 12.312EF^2 - 32.766EF^3) + 0.0006\Delta T) \tag{A.4}$$

where EF is the ratio of daily potential evapotranspiration to annual precipitation:

$$EF = \frac{\left(E_p/\rho_w\right)t_{day}}{l_{P,ann}}$$

and ρ_w is the density of water, 1000 kg m^{-3}, t_{day} is the length of daylight in seconds, $l_{P,ann}$ is the annual precipitation (mm), and the daily potential evapotranspiration E_p is estimated using the relation by Hargreaves and Samani (1985) :

$$E_p = S_0\left(0.0026\sqrt{\Delta T}\right)\left(T_{avg,C} + 17.8\right) \tag{A.5}$$

Appendix B

Statistical Inferences

NDVI-Canopy Cover

General population model: $y_i = \beta_0 + \beta x_i + \varepsilon_i$

β_0 *is the y intercept;*

β *is the slope; and*

ε_i *is the error*

Regression model: $\hat{y} = \beta_0 + \beta_1 x$

Hypotheses: $H_0: B_1 = 0;\ H_a: B_1 \neq 0$

Results and assumptions:

1. $E(\varepsilon_i) = 0$; Histogram of residuals is centered around 0 – Normal error distribution
2. $V(\varepsilon_i) = \sigma_\varepsilon^2$; No pattern
3. $Cov(\varepsilon_i, \varepsilon'_i) = 0$; DW statistic = **1.28**, less than 1.5 indicating slight positive autocorrelation;
4. $\varepsilon_i \sim N(0, \sigma_\varepsilon^2)$; qq plot light right skew– acceptable distribution

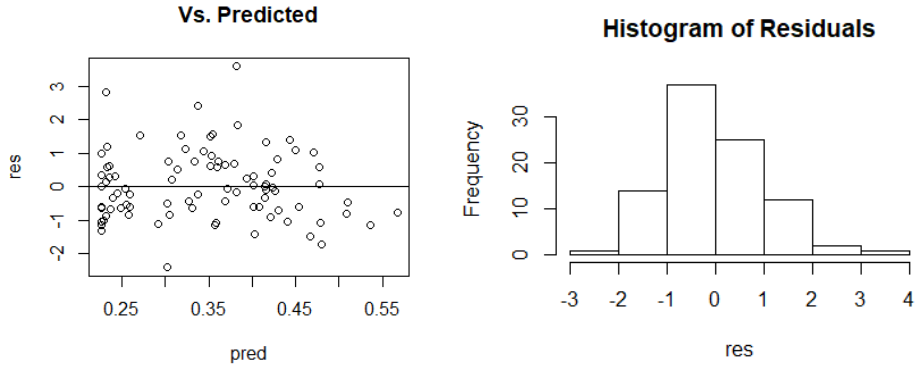

:

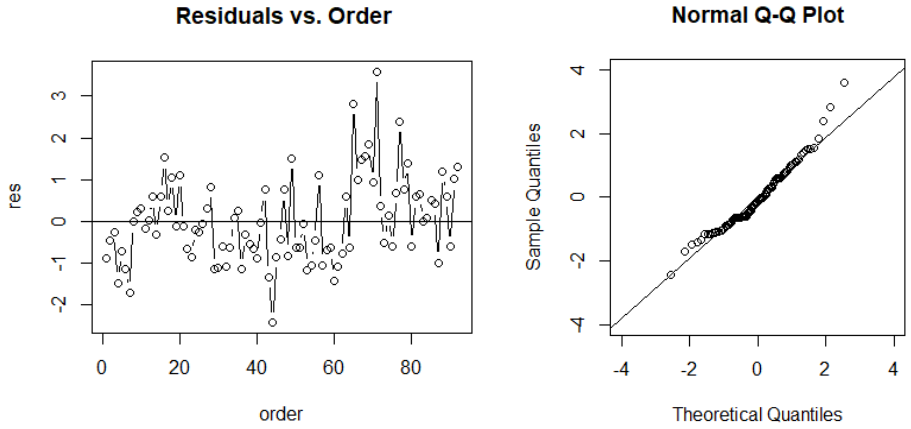

Regression Results:

```
Call:
lm(formula = NDVI ~ Obs_CC)
Residuals:
      Min        1Q    Median        3Q       Max
-0.156340 -0.043919 -0.008009  0.040642  0.223332
Coefficients:
            Estimate Std. Error t value Pr(>|t|)
(Intercept)  0.22572    0.01128   20.01   <2e-16 ***
Obs_CC       0.37802    0.02906   13.01   <2e-16 ***
Signif. codes:  0 ‘***’ 0.001 ‘**’ 0.01 ‘*’ 0.05 ‘.’ 0.1 ‘ ’ 1

Residual standard error: 0.06661 on 90 degrees of freedom
Multiple R-squared:  0.6529,     Adjusted R-squared:  0.649
F-statistic: 169.3 on 1 and 90 DF,  p-value: < 2.2e-16
```

Interpretation:

Assumptions are upheld, significance at $p < 0.001$, reject H_0, slope of the regression line between NDVI and canopy cover is significant.

Simulated vs Observed Canopy Cover

General population model: $y_i = \beta_0 + \beta x_i + \varepsilon_i$

β_0 *is the y intercept;*

β *is the slope; and*

ε_i *is the error*

Regression model: $\hat{y} = \beta_0 + \beta_1 x$

Hypotheses: $H_0: B_1 = 0;\ H_a: B_1 \neq 0$

Results and assumptions:

1. $E(\varepsilon_i) = 0$; Histogram of residuals is centered around 0 – Lightly skewed left
2. $V(\varepsilon_i) = \sigma_\varepsilon^2$; No pattern
3. $Cov(\varepsilon_i, \varepsilon'_i) = 0$; DW statistic = **2.30**, less than 2.5 indicating no autocorrelation;
4. $\varepsilon_i \sim N(0, \sigma_\varepsilon^2)$; qq plot light left tailing– acceptable distribution

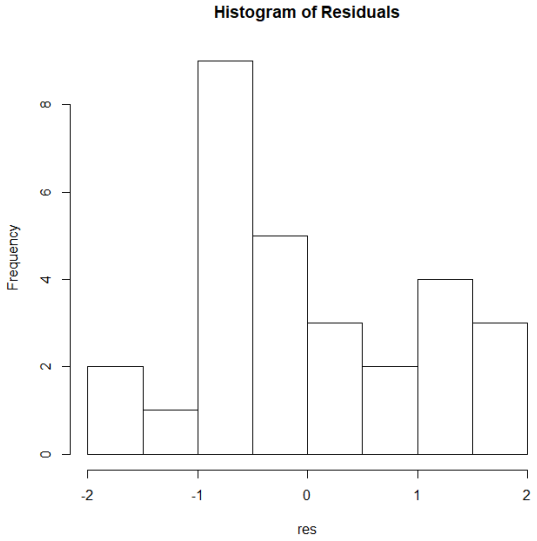

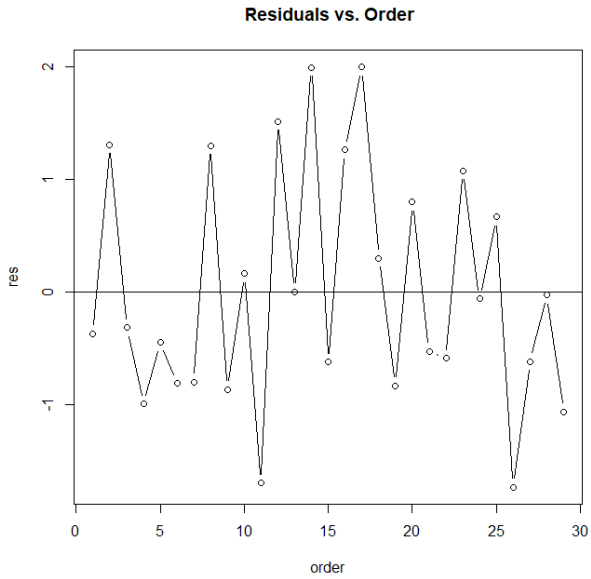

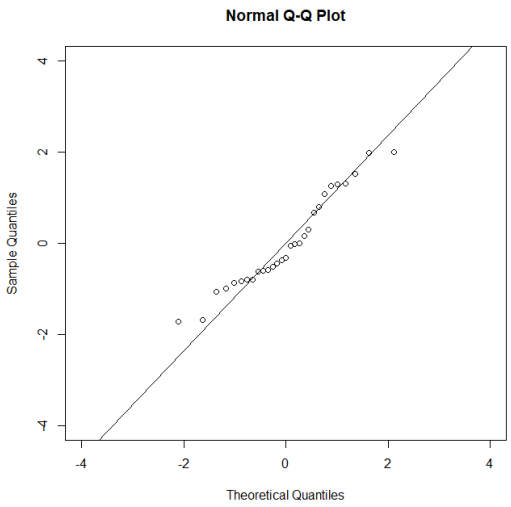

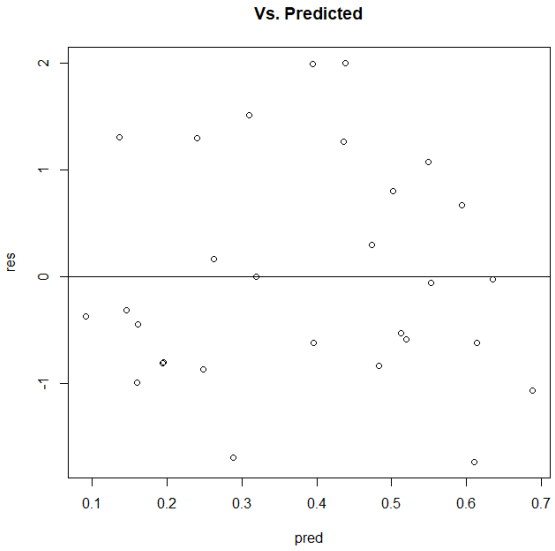

Regression results:

```
 Call:
lm(formula = sim ~ obs)

Residuals:
     Min       1Q   Median       3Q      Max
-0.18305 -0.08833 -0.03470  0.08982  0.21277

Coefficients:
            Estimate Std. Error t value Pr(>|t|)
(Intercept)  0.08787    0.04204   2.090   0.0462 *
obs          0.83082    0.10153   8.183 8.68e-09 ***
---
Signif. codes:  0 ‘***’ 0.001 ‘**’ 0.01 ‘*’ 0.05 ‘.’ 0.1 ‘ ’ 1

Residual standard error: 0.1145 on 27 degrees of freedom
Multiple R-squared:  0.7126,    Adjusted R-squared:  0.702
F-statistic: 66.96 on 1 and 27 DF,  p-value: 8.683e-09
```

Interpretation:

Assumptions are upheld, significance at $p < 0.001$, reject H_0. Slope of the regression line between simulated and observed and canopy cover is significant.

Appendix C

```
// example javascript to allow polygon selection
//     in openlayers
var selectedRegion = null;
// define new selection function
var select = new ol.interaction.Select();
map.addInteraction(select);
select.on('select', function(e) {
// define new selection function
selectedRegion = e.selected;
console.log(selectedRegion)
// get selected ID from layer
var id = selectedRegion[0]["O"]["ID"];
// update previously defined image object with new ID
$("#theimg").attr("src", "img/" + id + ".png");
});
```

Snippet 1. Sample JavaScript code to allow selection of polygon objects in OpenLayers and prompt change in some display feature. This example demonstrates changing a static image to the respective selected hillslope's 'ID' value.